FINAL REPORT

A. PROJECT DESCRIPTION

Date of this report : 5th July 2004

1. **Account No:** 304 – PFIZIK – 670011
2. **Project Title:** Hydrogen-bondings, Phase-transitions and Theoretical Studies of Phenol Amine Adducts
3. **Project Leader :** Prof. Fun Hoong Kun
4. **Co-researchers:** Prof. Junaidah Osman, Dr. Abdul Razak Ibrahim & Dr. Anwar Usman

RECEIVED
- 9 JUL 2004
UNIVERSITI SAINS MALAYSIA
RCMO

ELSEVIER
Computational Materials Science xxx (2004) xxx–xxx
COMPUTATIONAL
MATERIALS
SCIENCE
www.elsevier.com/locate/commatsci

Second harmonic generation from a ferroelectric film

R. Murgan, F. Razak, D.R. Tilley, T.Y. Tan, J. Osman *, M.N.A. Halif

School of Physics, Universiti Sains Malaysia, 11800 Penang, Malaysia

Received 12 December 2003; received in revised form 26 February 2004; accepted 5 March 2004

Abstract

We derive an expression for transmittivity (T_{SHG}) of second harmonic generation (SHG) signals from a ferroelectric (FE) film. Intensities of up and down fields in the medium are investigated in relation to T_{SHG}. The derivations are made based on undepletion of input fields and nonlinear wave equation derived from the Maxwell equations. We present two cases: film without mirrors and with partial mirrors. Expressions for the newly derived nonlinear susceptibility coefficients of SHG for real crystal symmetry [J. Opt. Soc. Am. B 19 (2002) 2007] are used to get more realistic results. Variations in T_{SHG} with respect to film thickness are illustrated.

PACS: 42.65.–k; 42.65.Ky; 77.84.–s
Keywords: Ferroelectrics; Second harmonic generation; Nonlinear optics; Susceptibility coefficients

1. Introduction

X-ray diffraction analysis is a common technique used to study a film structure prior to electrical characterization. However, when films get very thin, nonlinear second-harmonic generation (SHG) based technique is found to be more sensitive and gives better spatial resolution [1]. In 1996, Gopalan and Raj [2] developed a SHG technique to characterize domain structure of ferroelectrics (FE) films; and this technique was later used by Barad et al. [3].

Recently, Mishina et al. [4] develops a SHG technique for the structural characterization of domain structure of thin barium strontium titanate (BST) films. In order to understand their SHG measurements, they use the expressions of SHG nonlinear susceptibility tensor components derived theoretically by Osman et al. [5]. The work of Osman et al. [5] is based on the assumption that the FE crystal symmetry is uniaxial, which is just an approximate model of a FE crystal. A more accurate derivation of SHG tensor components is given recently by Rajan et al. [6] for real crystal symmetries like tetragonal and rhombohedral. We feel that the model used in [6] to derive the SHG coefficient expressions will give a more accurate explanation of their measurements and could provide a better fit to their data.

---

* Corresponding author. Tel.: +60-04-65-33655/77888; fax: +60-04-65-79150.
E-mail address: junaidah@usm.my (J. Osman).

0927-0256/$ - see front matter © 2004 Published by Elsevier B.V.
doi:10.1016/j.commatsci.2004.03.016

The aim of this paper therefore is to study the transmissivity, T_{SHG}, of SHG signals from a FE film using the SHG coefficient expressions derived in [6] in order to get more realistic results and to obtain a better understanding of the SHG mechanism occurring in a FE film. The derivations are made based on undepletion of input fields and nonlinear wave equation derived from the Maxwell equations. Here SHG waves generated are analyzed theoretically by taking the total output field as a linear combination of particular and homogenous solutions of an inhomogeneous nonlinear wave equation. The treatment presented here is similar to the formalism used by Bloembergen and Pershan [7] who first considered harmonic generation and wave mixing in the presence of plane interfaces. As an example of specific material, we choose $\mathrm{BaTiO_3}$ in its tetragonal phase ($T < T_c$), where T_c is the critical temperature; and various parameters of $\mathrm{BaTiO_3}$ based on Refs. [8,9] will be utilized in our model. We shall consider two cases: film without mirrors and with partial mirrors. To illustrate the numerical results, variations in T with respect to film thickness are illustrated.

Section 2 of this paper is devoted mainly to develop the required formalism, where essential differential equations are set up and solved analytically. In Section 3, we give some graphical illustrations of the results obtained together with discussions. This is followed by a brief conclusion in Section 4.

2. Formalism

We begin the formalism by considering a thin FE film of thickness L. SHG waves are assumed generated in the film with the input waves as the driving fields, considered undepleted in the weak nonlinearity regime. Here, we assume that the FE medium is anisotropic in its tetragonal phase ($T < T_c$) and has nonzero nonlinear susceptibility tensor element for SHG, $\chi^{\mathrm{SHG}}_{zzz}(-2\omega;\omega,\omega)$ [6]. In order to generate the SHG we therefore take the input waves polarized in the z direction and for simplicity assumed normally incident.

The geometry of the system is illustrated in Fig. 1. In principle under the undepleted input field approximation, the optics of the problem involves (1) a linear optics of reflection and transmission problem from the film involving amplitudes aE_0, bE_0, rE_0 and tE_0 representing down, up, reflected and transmitted waves, respectively; (2) a SHG reflection and transmission problem from the film involving amplitudes $\varphi_1 E_0$, $\varphi_2 E_0$, ρE_0 and τE_0, where they are the down, up, reflected and transmitted waves of the generated SHG waves, respectively. The coefficients a, b, r, t, φ_1, φ_2, ρ and

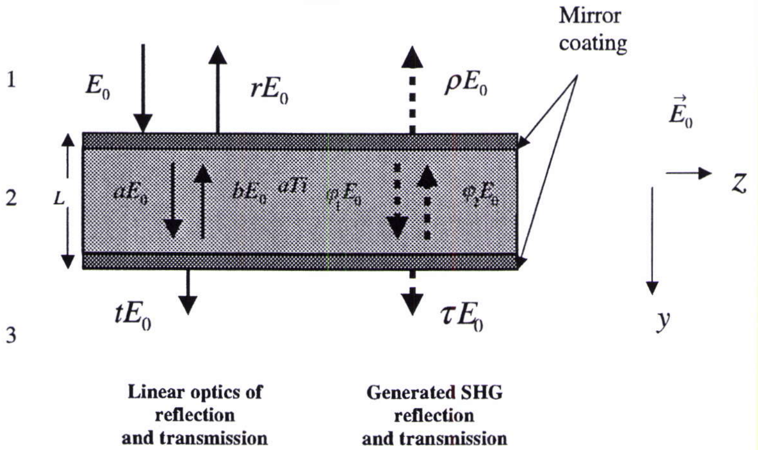

Fig. 1. Geometry of the problem showing the cross section of the FE film considered to be $\mathrm{BaTiO_3}$ with thickness L. The input field with amplitude $\vec{E}_0$ is assumed z polarized. In general, the number 1, 2, and 3 represent medium: 1 is the medium above the film, 2 the film medium, and 3 the medium below the film.

τ each refers to a fraction of an input field with an assumed amplitude E_0. The film medium is represented by the number 2, the number 1 is the medium above and 3 below, which in general may be air above and a substrate below.

The solutions of a, b, r and t are standard and can be found in any standard textbook on optics [10]. For completeness and clarity, the results are summarized below, in terms of the Landau–Liftshitz notations τ_{lm} and ρ_{lm}.

$$a = \frac{\tau_{12}}{1+(\delta_2)^2\rho_{12}\rho_{23}}, \quad b = \frac{\tau_{12}\rho_{23}(\delta_2)^2}{1+(\delta_2)^2\rho_{12}\rho_{23}}, \tag{1}$$

$$r = \frac{\tau_{21}\tau_{12}\rho_{21}-(\delta_2)^2\rho_{12}\rho_{23}-1}{\rho_{21}\left[1+(\delta_2)^2\rho_{12}\rho_{23}\right]}, \quad t = \frac{\tau_{23}\tau_{12}\delta_2}{\delta_3\left[1+(\delta_2)^2\rho_{12}\rho_{23}\right]}, \tag{2}$$

where

$$\rho_{lm} = \frac{k_l-k_m-\gamma}{k_l+k_m+\gamma}, \quad \tau_{lm} = \frac{2k_l}{k_l+k_m+\gamma} \quad (l,m=1,2,\text{ or }3). \tag{3}$$

In the above equations, $\delta_l = \exp(\mathrm{i}k_lL)$, $k_l=(\omega/c)\sqrt{\varepsilon_l}$, and γ represents a mirror term to include the possibility that the film may be coated with a mirror layer on both sides. The subscripts l and m refer generally to medium 1, 2, or 3. ε_1, ε_2 and ε_3 is the relative permittivity of medium 1, 2 and 3, respectively.

Assuming an input frequency, ω, the total fields above the film are

$$E_z^{(1)}(y,t) = E_0\left[\exp(\mathrm{i}k_1^{\omega}y) + r\exp(-\mathrm{i}k_1^{\omega}y)\right]\exp(-\mathrm{i}\omega t) + \rho E_0\exp(-\mathrm{i}k_1^{2\omega}y)\exp(-\mathrm{i}2\omega t) \tag{4a}$$

and

$$H_x^{(1)}(y,t) = (k_1^{\omega}/\omega\mu_0)E_0\left[\exp(\mathrm{i}k_1^{\omega}y) - r\exp(-\mathrm{i}k_1^{\omega}y)\right]\exp(-\mathrm{i}\omega t) + (k_1^{2\omega}/2\omega\mu_0)\rho E_0\exp(-\mathrm{i}k_1^{2\omega}y) \times \exp(-\mathrm{i}2\omega t), \tag{4b}$$

where $k_1^{\omega}=(\omega/c)\sqrt{\varepsilon_1^{\omega}}$ and $k_1^{2\omega}=(2\omega/c)\sqrt{\varepsilon_1^{2\omega}}$ is the propagation constant of the input field and the reflected SHG field, respectively. In general, the relative permittivity of medium 1, 2 or 3 is dispersive. Consequently, ε_1^{ω} and $\varepsilon_1^{2\omega}$ for example, denote the relative permittivity of medium 1 with each evaluated at frequency ω and 2ω, respectively.

The total fields below the film (medium 3) are

$$E_z^{(3)}(y,t) = tE_0\exp(\mathrm{i}k_3^{\omega}y)\exp(-\mathrm{i}\omega t) + \tau E_0\exp(\mathrm{i}k_3^{2\omega}y)\exp(-\mathrm{i}2\omega t) \tag{5a}$$

and

$$H_x^{(3)}(y,t) = (k_3^{\omega}/\omega\mu_0)tE_0\exp(\mathrm{i}k_3^{\omega}y)\exp(-\mathrm{i}\omega t) + (k_3^{2\omega}/2\omega\mu_0)\tau E_0\exp\left(\mathrm{i}k_3^{2\omega}y\right) \times \exp(-\mathrm{i}2\omega t), \tag{5b}$$

where $k_3^{\omega}=(\omega/c)\sqrt{\varepsilon_3^{\omega}}$ and $k_3^{2\omega}=(2\omega/c)\sqrt{\varepsilon_3^{2\omega}}$ are the propagation constant of the transmitted input and SHG field, respectively. Similarly, ε_3^{ω} and $\varepsilon_3^{2\omega}$ symbolize the relative permittivity of a medium 3 with each evaluated at frequency ω and 2ω, respectively. Since ε_1 and ε_3 are in general dispersive, then $\varepsilon_1^{\omega}\neq\varepsilon_1^{2\omega}$ and $\varepsilon_3^{\omega}\neq\varepsilon_3^{2\omega}$.

In order to solve for ρ and τ, we consider a nonlinear wave equation for the generated SHG wave propagating in the film medium, $\nabla^2\vec{E}-\mu_0\partial^2\vec{D}/\partial t^2=0$, where $\vec{D}=\varepsilon_0\vec{E}+\vec{P}^{\mathrm{L}}+\vec{P}^{\mathrm{NL}}$ with $\vec{P}^{\mathrm{L}}$ and $\vec{P}^{\mathrm{NL}}$ denoting linear and nonlinear polarization induced by the input fields. For z-polarized input field, we have

$$P_z^{\mathrm{L}} = \varepsilon_0\chi_{zz}^{(1)}E_z^{2\omega} \quad\text{and}\quad P_z^{\mathrm{NL}} = \varepsilon_0\chi_{zzz}^{\mathrm{SHG}}E_z^{\omega}E_z^{\omega}, \tag{6}$$

where $\chi_{zz}^{(1)}$ is the linear susceptibility and $\chi_{zzz}^{\mathrm{SHG}}$ the nonlinear susceptibility for SHG, which in general may be frequency-dependent. Here, E_z^{ω} and $E_z^{2\omega}$ represent the electric field of the input waves propagating at frequency ω and the generated SHG field propagating at frequency 2ω, respectively. In the film, we may write the electric field as

$$E_z^{\omega}(y,t) = (1/2)\left[aE_0\exp(\mathrm{i}k_2y)\exp(-\mathrm{i}\omega t) + a^*E_0^*\exp(-\mathrm{i}k_2y)\exp(\mathrm{i}\omega t) + bE_0\exp(-\mathrm{i}k_2y)\exp(-\mathrm{i}\omega t) + b^*E_0^*\exp(\mathrm{i}k_2y)\exp(\mathrm{i}\omega t)\right] \tag{7}$$

representing up and down waves, and we let the generated SHG field to have a form

$$E_z^{2\omega}(y,t) = (1/2)\left[\zeta(y)E_0\exp(-\mathrm{i}2\omega t) + \zeta^*(y)E_0^*\exp(\mathrm{i}2\omega t)\right]. \tag{8}$$

Substituting (7) and (8) into the nonlinear wave equation yields

$$\frac{\mathrm{d}^2\zeta}{\mathrm{d}y^2} + 4\frac{\omega^2}{c^2}\varepsilon_{zz}^{2\omega}\zeta(y) + 2\frac{\omega^2}{c^2}E_0\chi_{zzz}^{\mathrm{SHG}} [(a^2\mathrm{e}^{\mathrm{i}2k_2^{\omega}y} + b^2\mathrm{e}^{-\mathrm{i}2k_2^{\omega}y} + 2ab)] = 0, \tag{9}$$

where in (9), we use $\varepsilon_{zz}^{2\omega} = 1 + \chi_{zz}^{2\omega}$. $\chi_{zz}^{2\omega}$ and thus $\varepsilon_{zz}^{2\omega}$ denotes the value of $\chi_{zz}^{(1)}$ evaluated at frequency 2ω. By noting that

$$(k_2^{2\omega})^2 = \frac{4\omega^2}{c^2}\varepsilon_{zz}^{2\omega}, \tag{10}$$

two cases may be considered: (1) nonphase matching where $k_2^{2\omega} \neq 2k_2^{\omega}$, and (2) phase matching where $k_2^{2\omega} = 2k_2^{\omega}$. However, here we focus only on the former.

Subsequently, we seek solution of (9) under the nonphase matching condition. Using the standard method of undetermined coefficients, we obtain

$$\zeta(y) = \varphi_1\mathrm{e}^{\mathrm{i}k_2^{2\omega}y} + \varphi_2\mathrm{e}^{-\mathrm{i}k_2^{2\omega}y} + \sigma_{\mathrm{AB}}^2 + \sigma_{\mathrm{B}}^2\mathrm{e}^{-\mathrm{i}2k_2^{\omega}y} + \sigma_{\mathrm{A}}^2\mathrm{e}^{\mathrm{i}2k_2^{\omega}y}, \tag{11}$$

where

$$\sigma_{\mathrm{AB}}^2 = \left(-2\frac{\omega^2}{c^2}E_0\chi_{zzz}^{\mathrm{SHG}}ab\right)(k_2^{2\omega})^{-2}, \tag{12a}$$

$$\sigma_{\mathrm{A}}^2 = \left(-\frac{\omega^2}{c^2}E_0\chi_{zzz}^{\mathrm{SHG}}a^2\right)\left((k_2^{2\omega})^2 - 4(k_2^{\omega})^2\right)^{-1}, \tag{12b}$$

$$\sigma_{\mathrm{B}}^2 = \left(-\frac{\omega^2}{c^2}E_0\chi_{zzz}^{\mathrm{SHG}}b^2\right)\left((k_2^{2\omega})^2 - 4(k_2^{\omega})^2\right)^{-1}. \tag{12c}$$

These are known parameters with values obtained using (1) and (3). φ_1 and φ_2 are coefficients of the complementary solutions of (9). From (11), all the generated SHG fields within the film may be obtained. Using the fields expressed in (4) and (5), and the fields obtained from (11), application of standard electromagnetic boundary conditions at $y = 0$ and L gives a set of simultaneous equations, which may be written in matrix form as

$$\begin{bmatrix} -1 & -1 & 1 & 0 \\ -k_2^{2\omega} & k_2^{2\omega} & -k_1^{2\omega} & 0 \\ \delta_2^{2\omega} & (\delta_2^{2\omega})^* & 0 & -\delta_1^{2\omega} \\ k_2^{2\omega}\delta_2^{2\omega} & -k_2^{2\omega}(\delta_2^{2\omega})^* & 0 & -k_1^{2\omega}\delta_1^{2\omega} \end{bmatrix} \begin{bmatrix} \varphi_1 \\ \varphi_2 \\ \rho \\ \tau \end{bmatrix} = \begin{bmatrix} s_1 \\ s_2 \\ s_3 \\ s_4 \end{bmatrix}, \tag{13}$$

where

$$s_1 = \sigma_{\mathrm{AB}}^2 + \sigma_{\mathrm{A}}^2 + \sigma_{\mathrm{B}}^2, \tag{14a}$$

$$s_2 = -2\sigma_{\mathrm{B}}^2k_2^{\omega} + 2\sigma_{\mathrm{A}}^2k_2^{\omega}, \tag{14b}$$

$$s_3 = -\sigma_{\mathrm{AB}}^2 - \sigma_{\mathrm{A}}^2\delta_2^{\omega} - \sigma_{\mathrm{B}}^2(\delta_2^{\omega})^*, \tag{14c}$$

$$s_4 = 2[-\sigma_{\mathrm{A}}^2\delta_2^{\omega} + \sigma_{\mathrm{B}}^2(\delta_2^{\omega})^*]k_2^{\omega}. \tag{14d}$$

The above equations contain the following phase factors: $\delta_2^{2\omega} = \exp(\mathrm{i}k_2^{2\omega}L)$, $\delta_1^{2\omega} = \exp(\mathrm{i}k_1^{2\omega}L)$, and $\delta_2^{\omega} = \exp(\mathrm{i}2k_2^{\omega}L)$. Solutions of (13) yield the following coefficients for the generated SHG waves:

$$\rho = \frac{(k_2^{2\omega}s_1 + s_2) + 2k_2^{2\omega}\varphi_1}{-(k_1^{2\omega} - k_2^{2\omega})}, \tag{15}$$

$$\tau = \frac{(k_2^{2\omega}s_3 + s_4) - 2k_2^{2\omega}\delta_2^{2\omega}\varphi_1}{-(k_1^{2\omega} + k_2^{2\omega})\delta_1^{2\omega}}. \tag{16}$$

(15) and (16) is the reflection and transmission coefficient of the generated SHG waves, respectively with

$$\varphi_1 = \frac{-(\delta_2^{2\omega})^*(k_2^{2\omega} + k_1^{2\omega})(k_1^{2\omega}s_1 + s_2) + (k_1^{2\omega} - k_2^{2\omega})(s_4 - k_1^{2\omega}s_3)}{(\delta_2^{2\omega})^*(k_1^{2\omega} + k_2^{2\omega})^2 - \delta_2^{2\omega}(k_1^{2\omega} - k_2^{2\omega})^2} \tag{17a}$$

and for completeness

$$\varphi_2 = \frac{-(k_1^{2\omega} - k_2^{2\omega})(s_4 - k_1^{2\omega}s_3) - \delta_2^{2\omega}(k_2^{2\omega} - k_1^{2\omega})(k_1^{2\omega}s_1 + s_2)}{(\delta_2^{2\omega})^*(k_1^{2\omega} + k_2^{2\omega})^2 - \delta_2^{2\omega}(k_1^{2\alpha} - k_2^{2\omega})}. \tag{17b}$$

3. Results and discussion

The generation of SHG signal from the FE film may be understood by first studying the behavior of $\chi_{zz}^{(1)}$ and χ_{zzz}^{SHG}. Here, we use the expressions of $\chi_{zz}^{(1)}$ and χ_{zzz}^{SHG} for a FE material with tetragonal symmetry given by Ref. [6] which are

$$\chi_{zz}^{(1)} = \left[\varepsilon_0\left(-m\omega^2 - i\eta\omega - \frac{\alpha}{\varepsilon_0} + \frac{3\beta_1}{\varepsilon_0^2}P_0^2\right)\right]^{-1}, \qquad (18)$$

$$\chi_{zzz}^{SHG}(\omega) = -3\beta_1 P_0 s(2\omega)s^2(\omega), \qquad (19)$$

where $\alpha = a_0(T_c - T)$ with a_0 as the Curie constant, η, m and β_1 are material-dependent parameters, and $P_0 = \sqrt{a_0(T_c - T)\varepsilon_0/\beta_1}$ is the spontaneous polarization. Calculated values of these parameters, based on experimental values of Ref. [11], for BaTiO$_3$ are as follows: $m \sim 6.44\times10^{-21}$ kg m^3 s^{-2} A^{-2}, $\eta \sim 3.32\times10^{-5}$ kg m^3 s^{-1} A^{-2}, $P_0 \sim 0.1945$ Cm^{-2}, $\alpha \sim 5.22\times10^{-4}$ (for $T = 393$ K), and $\beta_1 \sim 1.913\times10^{-13}$ m^3 J^{-1}. The functions $s(\omega)$ and $s(2\omega)$ in (19) are the FE response functions [6] which have the form

$$s(n\omega) = \left[\left(-mn^2\omega^2 - i\eta n\omega - \frac{\alpha}{\varepsilon_0} + \frac{3\beta_1}{\varepsilon_0^2}P_0^2\right)\right]^{-1}, \quad n = 1, 2. \qquad (20)$$

Figs. 2 and 3 illustrate the behavior of real and imaginary parts of $\chi_{zz}^{(1)}$ and χ_{zzz}^{SHG} at temperature $T = 393$ K versus frequency, respectively, using the values of the parameters listed above. As expected for a FE material like BaTiO$_3$, both Re($\chi_{zz}^{(1)}$) and Re(χ_{zzz}^{SHG}) have very high values, for example at resonance Re($\chi_{zz}^{(1)}$) ≈ 250 and the value of Re(χ_{zzz}^{SHG}) is in the range 10^{-6} mV^{-1}. In comparison, a typical nonlinear optical material like LiNbO$_3$ has a value of Re($\chi_{zz}^{(1)}$) < 10 and Re(χ_{zzz}^{SHG}) $\approx 10^{-11}$ mV^{-1} [12]. The resonant frequency of $\chi_{zz}^{(1)}$ at $T = 393$ K is calculated to be around $\omega_0 \cong 5 \times 10^{12}$ Hz and χ_{zzz}^{SHG} is resonant when the denominator of (20) is zero. Note that the curves are rounded at resonances due to the large damping parameter used in the numerical calculation.

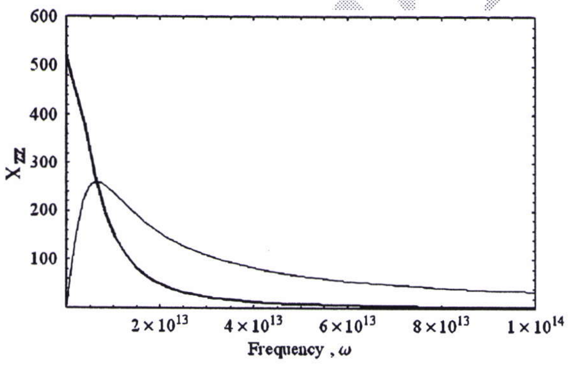

Fig. 2. The graph of Re(χ_{zz}) and Im(χ_{zz}) versus frequency, ω, at temperature $T = 393$ K using parameters for BaTiO$_3$. Thicker line: Re(χ_{zz}). Thinner line: Im(χ_{zz}).

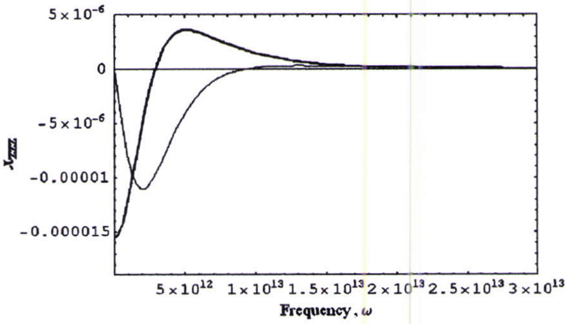

Fig. 3. The graph of Re(χ_{zzz}) and Im(χ_{zzz}) versus frequency, ω, at temperature $T = 393$ K using parameters for BaTiO$_3$. Thicker line: Re(χ_{zzz}). Thinner line: Im(χ_{zzz}).

Here we concentrate on an input frequency $\omega_1 = 1.5 \times 10^{13}$ Hz where as shown by Fig. 2, it is away from resonance, and consider the generation of SHG signal at frequency $2\omega_1 = 3.0 \times 10^{13}$ Hz. Fig. 4(a) and (b) shows the transmission curve of the generated SHG versus film thickness for film without mirror and with 90% mirror reflectivity. There exists a high peak demonstrating appreciable transmittance at a particular film thickness for both cases with and without mirror. As expected the transmissivity is much lower in magnitude for the case with mirror since here most of the input waves are reflected back into medium 1. The film thickness appears to be in the submicron range. At this film thickness, it is expected that there exists an almost complete constructive interference between the input waves propagating in the film at frequency $\omega_1 = 1.5 \times 10^{13}$ with the generated SHG waves propagating at frequency $2\omega_1$ [13].

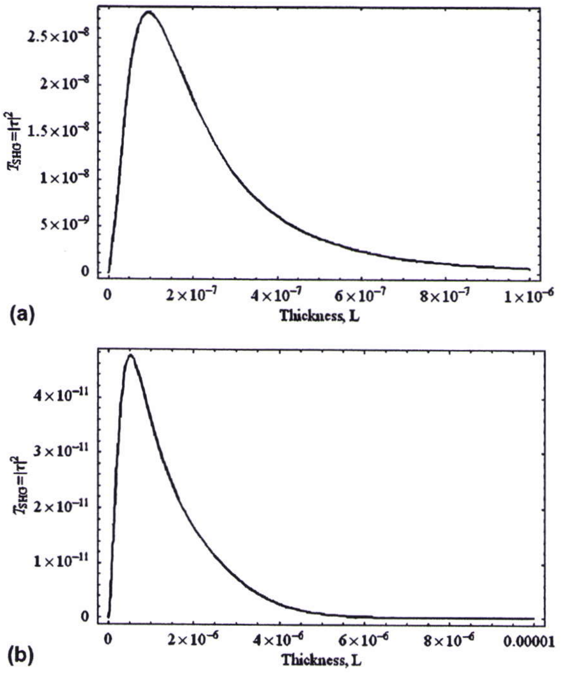

Fig. 4. Graphs of SHG transmission, $T_{\mathrm{SHG}} = |\tau|^2$, versus film thickness: (a) without mirror, and (b) with 90% mirror reflectivity. The frequency of the input field is assumed to be $\omega_1 = 1.5 \times 10^{13}$ Hz.

The value of T_{SHG} generated is small as expected since the formalism is based on weak nonlinearity (undepletion of the input waves) and phase mismatch condition.

4. Conclusion

We have analyzed SHG wave transmittivity through a FE film, based on standard nonlinear optics approach. We have given a full account on the behavior of SHG wave transmittivity for a film with and without mirror. In this work, we have used expressions of $\chi^{(1)}_{zz}$ and $\chi^{\mathrm{SHG}}_{zzz}$ in the tetragonal symmetry, concentrate only on z polarized input waves, and have specifically used $\mathrm{BaTiO_3}$ parameters in the numerical calculation. The work can be further extended to include the study of generated SHG signals using other nonvanishing SHG susceptibility tensor components, other symmetry like rhombohedral [6], and other type of FE material for example BST.

We have shown that the SHG signal is generated at submicron film thickness, thus substantiating the reason for the suitability of using SHG technique in studying FE crystal domain structure. We hope the results presented here can provide a better understanding and explanation of SHG mechanism and future SHG technique measurements.

Acknowledgements

This work is supported by the USM Fundamental Research Grant (No: 304.PFIZIK.600710).

References

[1] D.J. Bottomley, G. Lupke, J.G. Mihaychuk, H.M. van Driel, J. Appl. Phys. 74 (1993) 6072.
[2] V. Gopalan, R. Raj, Appl. Phys. Lett. 68 (1996) 1323.
[3] Y. Barad, J. Lettieri, C.D. Theis, D.G. Schlom, V. Gopalan, J.C. Jiang, X.Q. Pan, Appl. Phys. Lett. 89 (2001) 1387.
[4] E.D. Mishina, N.E. Sherstyuk, D. Barsky, A.S. Sigov, Yu.I. Golovko, V.M. Mukhorotov, M. De Santo, Th. Rasing, J. Appl. Phys. 93 (2003) 6216.
[5] J. Osman, Y. Ishibashi, D.R. Tilley, Jpn. J. Appl. Phys. 37 (1998) 4887.
[6] R. Murgan, D.R. Tilley, Y. Ishibashi, J.F. Webb, J. Osman, J. Opt. Soc. Am. B 19 (2002) 2007.
[7] N. Bloembergen, P.S. Pershan, Phys. Rev. 128 (1962) 606.
[8] I. Frederov, J. Petzelt, V. Železný, G.A. Komandin, A.A. Volkov, K. Brooks, Y. Huang, N. Setter, J. Phys.: Condens. Matter 7 (1995) 4313.
[9] F. Razak, J.F. Webb, R. Murgan, Y. Ishibashi, J. Osman, Ferroelectrics 273 (2002) 2557.
[10] M. Born, E. Wolf, Principle of Optics: Electromagnetic Theory of Propagation Interference and Diffraction of Light, sixth ed., Pergamon Press, Oxford, 1980.
[11] Y.G. Wang, W.L. Zhong, P.L. Zhang, Solid State Commun. 92 (1994) 519.
[12] Y.R. Shen, The Principle of Nonlinear Optics, Wiley, New York, 1984.
[13] R. Murgan, D.R. Tilley, J. Osman, M.N.A Halif, Second-harmonic generation (SHG) in commensurate and incommensurate materials, in: Proceeding National Physics Conference PERFIK 2003, Fraser Hill, Malaysia, August 2003.

PERGAMON

Available online at www.sciencedirect.com
SCIENCE @ DIRECT®

Solid State Communications 127 (2003) 677–682

solid
state
communications

www.elsevier.com/locate/ssc

Phase transitions in hydrogen-bonded phenol–amine adducts: analysis by ferroelastic theory

H.-K. Fun[a,*], A. Usman[a], S. Chantrapromma[a,b], J. Osman[a], L.-H. Ong[a], D.R. Tilley[a], Y. Ishibashi[c]

[a]*School of Physics, Universiti Sains Malaysia, 11800 USM Penang, Malaysia*
[b]*Department of Chemistry, Faculty of Science, Prince of Songkla University, Hat-Yai, Songkla 90112, Thailand*
[c]*Faculty of Communications, Aichi Shukutoku University, Nagakute-cho, Aichi Prefecture 480-1197, Japan*

Received 20 May 2003; accepted 20 June 2003 by R.T. Phillips

PERGAMON

Available online at www.sciencedirect.com
SCIENCE DIRECT

Solid State Communications 127 (2003) 677–682

solid
state
communications

www.elsevier.com/locate/ssc

Phase transitions in hydrogen-bonded phenol–amine adducts: analysis by ferroelastic theory

H.-K. Fun[a,*], A. Usman[a], S. Chantrapromma[a,b], J. Osman[a], L.-H. Ong[a], D.R. Tilley[a], Y. Ishibashi[c]

[a] *School of Physics, Universiti Sains Malaysia, 11800 USM Penang, Malaysia*
[b] *Department of Chemistry, Faculty of Science, Prince of Songkhla University, Hat-Yai, Songkhla 90112, Thailand*
[c] *Faculty of Communications, Aichi Shukutoka University, Nagakute-cho, Aichi Prefecture 480-1197, Japan*

Received 20 May 2003; accepted 20 June 2003 by R.T. Phillips

Abstract

Phase transitions in a recently discovered class of hydrogen-bonded organic crystals are analyzed by Landau theory. It is shown that the transitions are ferroelastic. Two types of transition, orthorhombic-to-monoclinic and monoclinic-to-triclinic, are analysed using an expansion of the free energy in symmetry-allowed powers of the strain components. For three examples, new data are presented for the crystallographic parameters in a range of temperature including the phase transition point T_c. These data show that the transitions are second order and the temperature dependences are consistent with the mean-field analysis. We propose that the making and breaking of the hydrogen bond interactions with variation of temperature accounts for these reversible ferroelastic phase transitions. Expressions are derived for the entropy and the specific-heat discontinuity at T_c. It is pointed out that the transitions should be accompanied by 'soft-mode' behavior in a phonon of appropriate symmetry.

PACS: 61.50.Ks; 64.70. − p; 64.70.Kb

Keywords: A. Organic crystals; A. Ferroelastic; D. Phase transitions; D. Landau theory

---

1. Introduction

Interactions between phenols, compounds having at least one hydroxyl group, and amines, compounds having at least one amino group, are important in biological systems [1]. The phenols and amines are acidic and basic compounds, respectively. Solid crystals containing phenols and amines, so called phenol–amine adducts, are also widely used to study hydrogen bonds since the two components are generally linked by intermolecular O–H···O, O–H···N or N–H···O types of hydrogen bonds which are among the most robust and versatile synthons in crystal engineering [2, 3]. Owing to this interest, we have recently synthesized in crystalline form a number of the phenol–amine adducts with phenols of different acidity and with amines ranging from primary to tertiary, corresponding to the amino group having two to zero hydrogen atoms, and we have reported their crystal structure analyses [4–11]. We found that the behavior of the amine base in adducts is co-related to the possible H-transfer from the phenol counter part. As an example, we schematically show in Scheme 1 the structure of our compound **I**, in which the amine is a cation and the phenol is an anion. The broken lines in the scheme denote the intermolecular N–H···O hydrogen bonds. We may use benzoic acid, instead of phenol, to form salt-like adducts with similar intermolecular hydrogen bond types, in which the acid also readily forms an anion with the H-transfer process.

In crystalline form, these adducts form additional intermolecular hydrogen bonds amongst one another.

---

[*] Corresponding author. Tel.: +81-604-6533888x3690; fax: +81-604-6579150.
E-mail address: hkfun@usm.my (H.K. Fun).

doi:10.1016/S0038-1098(03)00516-7

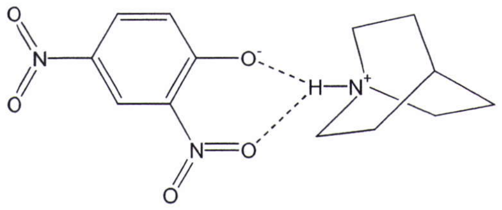

Scheme 1. Schematic diagram of compound **I**.

These intermolecular hydrogen bonds are part of the interactions that pack these adducts in regular arrangements in the crystals.

With changing temperature, some of the phenol–amine adducts undergo a distortive reversible phase transition, in some cases orthorhombic-to-monoclinic [9,11] and in others monoclinic-to-triclinic [4]. Here we present further data on the changes of the unit-cell parameters through the phase-transition region. We present expansions for the ferroelastic free energy in terms of the relevant lattice strains, derive expressions for measured quantities and show that the temperature dependences of unit cell parameters are consistent with our mean-field analysis.

The data presented in Figs. 2 and 3 are collected using a Bruker SMART 1K CCD diffractometer whereas the data of Fig. 5 were collected using a Nonius Kappa CCD 1K diffractometer. Both CCD diffractometers were equipped with low-temperature attachments. These cell parameters were measured in the standard manner as normally used for single-crystal x-ray structure determination. Caution was taken that thermal equilibrium has been achieved at each temperature before the data were collected.

2. Orthorhombic-to-monoclinic transitions: quinuclidinium-2,4-dinitrophenolate (I) and hexamethylenetetraminium-3,5-dinitrobenzoate-3,5-dinitrobenzoic acid monohydrate (II)

The crystallographic data for **I** (Scheme 1) and **II** (Scheme 2) show that at the critical temperature T_c the orthorhombic c axis tilts away from the vertical to the a–b plane (Fig. 1). The rotation is in the a–c plane so that the b axis remains normal to the a–c plane. This is consistent with the space group transformation $P_{bca} \rightarrow P_{2_1/c}$. Experimental data for the temperature dependence of the unit-cell parameters are shown in Figs. 2 and 3. Both phase transitions occur at approximately $T_c = 220$ K where β starts to change from the orthorhombic value of 90°. The data are consistent with the temperature dependences $\Delta\beta \propto (T_C - T)^{1/2}$ and $\Delta\ell \propto T_C - T$ where ℓ is a, b or c; as shown below, these results follow from mean-field theory.

We analyze the transition by the Landau form of mean-field theory for ferroelastic transitions. We expand the free energy in terms of the strain components, denoted as u_α, where $\alpha \equiv ij$ with $1 \equiv xx$, $2 \equiv yy$, $3 \equiv zz$, $4 \equiv yz$, $5 \equiv zx$ and $6 \equiv xy$. The strains are taken relative to the high-temperature orthorhombic phase. The primary order parameter is $u_5 \equiv u_{zx}$ and u_5 is a function of β, with $u_5 \propto (\beta - \pi/2)$ for small $(\beta - \pi/2)$. We take the free energy as

$$f - f_0(T) = \frac{c_{55}^{(0)}}{2}u_5^2 + \frac{\xi'}{4}u_5^4 + (\gamma_1 u_1 + \gamma_2 u_2 + \gamma_3 u_3)u_5^2 + \frac{c_{11}^{(0)}}{2}u_1^2 + \frac{c_{22}^{(0)}}{2}u_2^2 + \frac{c_{33}^{(0)}}{2}u_3^2 \quad (1)$$

where $f_0(T)$ is the non-ferroelastic part and cross terms in u_1u_2, u_2u_3 and u_1u_3 are omitted for simplicity. The first two terms in (1) are the lowest-order, symmetry-allowed, powers of u_5 and in order to describe the phase transition we take $c_{55}^{(0)} = C(T - T_C)$ since the phase transition point is given by $c_{55}^{(0)} = 0$. The third term in (1) is the lowest-order coupling between u_5 and the diagonal strain components and the final three terms are the quadratic elastic energy. The mean-field equilibrium values of the strain components correspond to a minimum of f. It is convenient to eliminate u_1, u_2 and u_3; since

$$\frac{\partial f}{\partial u_i} = c_{ii}^{(0)}u_i + \gamma_i u_5^2 = 0 \quad (2)$$

we find

$$u_i = -\frac{\gamma_i}{c_{ii}^{(0)}}u_5^2 \quad (3)$$

where $i = 1, 2, 3$. Eq. (3) can be substituted into (1) to give an expression for f in terms of u_5 alone:

$$f - f_0(T) = \frac{c_{55}^{(0)}}{2}u_5^2 + \frac{\xi}{4}u_5^4 \quad (4)$$

where

$$\xi = \xi' - 2\left(\frac{\gamma_1^2}{c_{11}^{(0)}} + \frac{\gamma_2^2}{c_{22}^{(0)}} + \frac{\gamma_3^2}{c_{33}^{(0)}}\right) \quad (5)$$

Eq. (4) is a simple Landau expansion. On the assumption that $c_{55}^{(0)}$ is linear in T, as mentioned before, and that the other coefficients in (1) are independent of T it leads to the temperature dependences of the various measured quantities for **I** and **II**, as will now be shown. The mean-field equilibrium state is the value of u_5 that minimizes f, and from (4) for $T < T_C$ this is

$$u_5 = C^{1/2}(T_C - T)^{1/2}/\xi^{1/2} \quad (6)$$

This equation agrees with Figs. 2(b) and 3(b) in which $\Delta\beta \propto (T_C - T)^{1/2}$. Introducing (6) into (3), we see that the changes in the lattice parameters, which are proportional to u_1, u_2 and u_3, are therefore proportional to $T_C - T$. This is consistent with Figs. 2(a) and 3(a).

The phase transition that has been discussed above is typical of the orthorhombic-to-monoclinic transitions in this class of compounds and we have shown that the experimental data agree with the mean-field predictions.

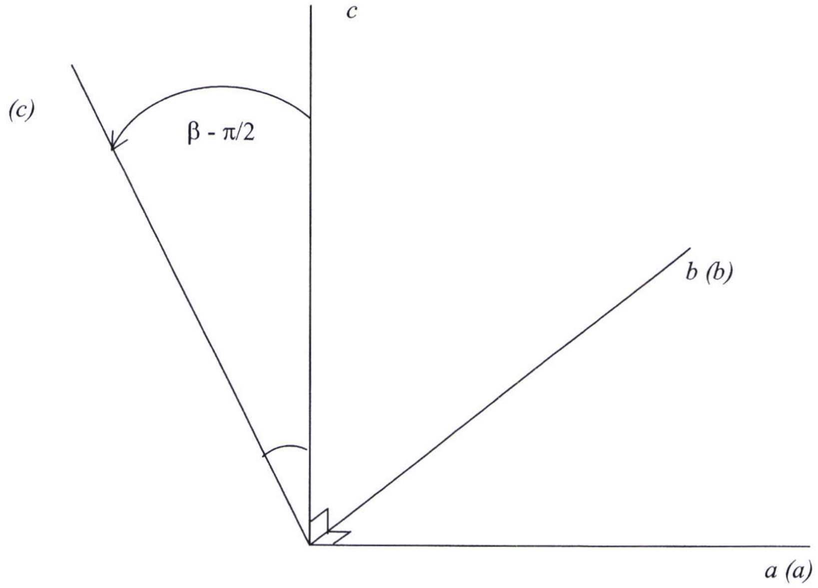

Fig. 1. A sketch showing the orthorhombic to monoclinic phase transition. The axes are labelled for the orthorhombic phase, with the monoclinic axis labels shown in brackets.

3. Monoclinic-to-triclinic transition: Hexamethylenetetraminium 2,4-dinitrophenolate monohydrate (III)

The crystallographic data of **III** (Scheme 3) indicate that the crystal is monoclinic at room temperature and triclinic at 143 K [4]. Data presented below show that the phase transition occurs at $T_C \approx 260$ K and that below the phase transition the monoclinic b axis rotates away from 90° in the plane while remaining almost perpendicular to the a axis, as sketched in Fig. 4. Because of the crystallographic conventions, the axis labels change in the phase transition according to $a \rightarrow -(b)$, $b \rightarrow +(a)$, and $c \rightarrow (c)$, as indicated in Fig. 4. This is consistent with the space group transformation $P_{2_1/m} \rightarrow P\bar{1}$ [4].

We now show, in Fig. 5, the crystallographic results for the temperature dependence of the unit-cell parameters. We start with the angles. First note that the apparent jump in monoclinic angle β is not a jump at all; it is simply the change $\beta \rightarrow (\alpha) = \pi - \beta$ resulting from the crystallographic convention. Second, it is seen that β remains very close to 95° and γ remains very close to 90°. The angle α or (β) changes abruptly from 90° around T_c and continuously moves away from 90° as T falls below T_c. These changes in the angles lead to the interpretation of the phase transition shown in Fig. 4. The six plots for the lattice parameters shown in Fig. 5, excepting the discontinuities around T_c, show very small changes in a, c, β and γ and with a temperature dependence for b or (a) and α or (β) which is consistent with a mean-field linear prediction.

These data are consistent with an analysis similar to that of Section 2. In view of the temperature dependence of α (Fig. 5b), the primary order parameter is $u_4 \equiv u_{yz}$ since u_4 is

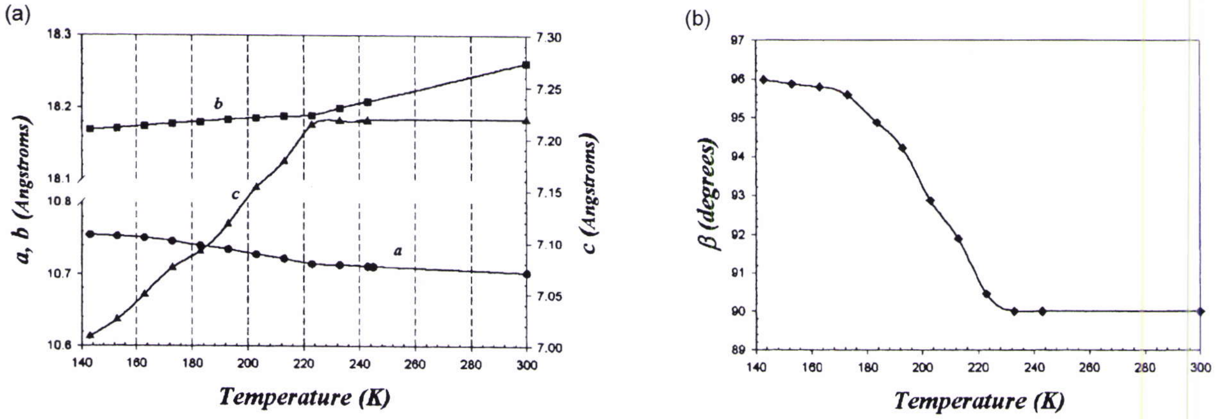

Fig. 2. Temperature dependences of unit-cell parameters of **I**. (a) Unit-cell lengths (b) angle β.

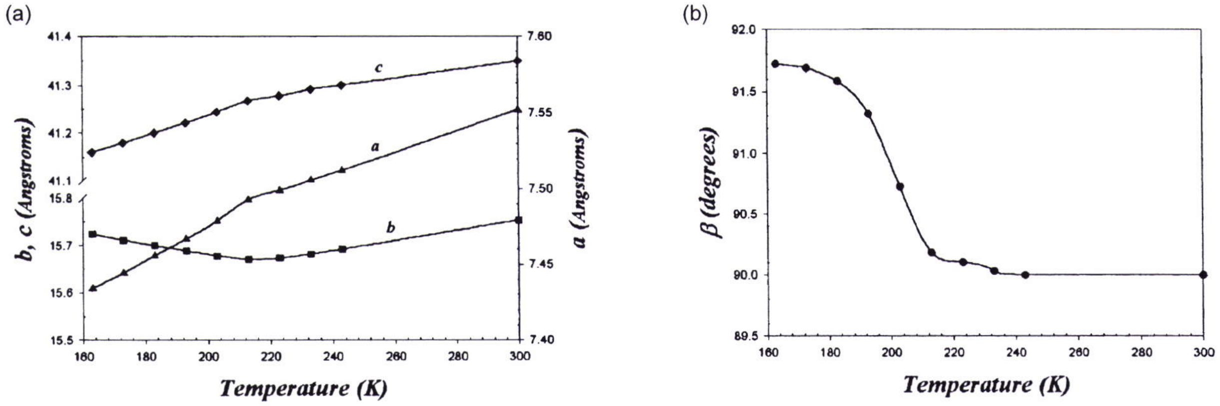

Fig. 3. Temperature dependences of unit-cell parameters of **II**. (a) Unit-cell lengths, (b) angle β.

a function of α with $u_4 \propto (\alpha - \pi/2)$ for small $\alpha - \pi/2$. Since the angle γ does not remain exactly equal to 90° we also include $u_6 \equiv u_{xy}$ as an order parameter; it is related to γ in the same way as u_4 is related to α. Our form for the free energy is therefore

$$f - f_0(T) = \frac{c_{44}^{(0)}}{2} u_4^2 + \frac{\xi'}{4} u_4^4 + c_{46}^{(0)} u_4 u_6 + \frac{c_{66}^{(0)}}{2} u_6^2 + \frac{\xi''}{4} u_6^4 + (\gamma_1 u_1 + \gamma_2 u_2 + \gamma_3 u_3) u_4^2 + \frac{c_{11}^{(0)}}{2} u_1^2 + \frac{c_{22}^{(0)}}{2} \times u_2^2 + \frac{c_{33}^{(0)}}{2} u_3^2 \tag{7}$$

where cross terms in u_1u_2, u_2u_3 and u_1u_3 are omitted for simplicity. Of course the coefficients in (7) do not have the same numerical value as those denoted by the same symbols in (1).

Eq. (7) may be analyzed in a similar way to (1). First, minimizing with respect to u_6 we find

$$\xi'' u_6^3 + c_{66}^{(0)} u_6 + c_{46}^{(0)} u_4 = 0 \tag{8}$$

from which it follows that if the coefficients $c_{46}^{(0)}$ and $c_{66}^{(0)}$ are not temperature dependent then u_6 has the same temperature dependence as u_4 for small ξ''. Clearly to account for the very weak temperature dependence for γ (Fig. 5b) requires $c_{66}^{(0)} \gg c_{44}^{(0)}$. The strains u_1, u_2 and u_3 are given by relations of the form of (3) with u_4 replacing u_5. Substitution of these forms in (7) together with (8) leads to

$$f - f_0(T) = \frac{1}{2}\left(c_{44}^{(0)} - \frac{\left(c_{46}^{(0)}\right)^2}{c_{66}^{(0)}} \right) u_4^2 + \frac{\xi}{4} u_4^4 \tag{9}$$

where ξ is given as in (5).

We now follow the discussion of Section 2. We assume the temperature dependence

$$c_{44}^{(0)} - \frac{(c_{46}^{(0)})^2}{c_{66}^{(0)}} = B(T - T_C) \tag{10}$$

and we then find $u_4 = B^{1/2}(T_C - T)^{1/2}/\beta^{1/2}$. This leads to similar temperature dependences to those of Section 2, namely $\Delta\alpha \propto (T_C - T)^{1/2}$, and $\Delta b \propto T_C - T$. These results are consistent with the data shown in Fig. 5.

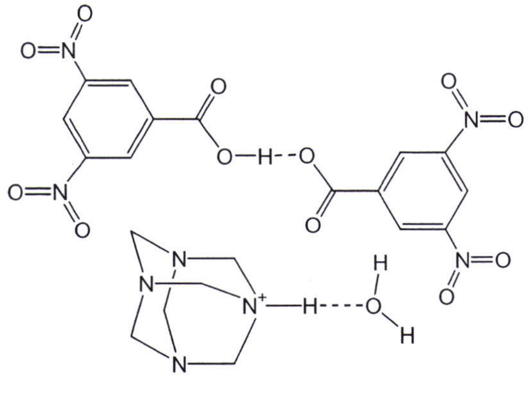

Scheme 2. Schematic diagram of compound **II**.

4. Conclusions

We have presented new data concerning the phase transitions in some novel hydrogen-bonded phenol–amine adducts and shown that they are consistent with a mean-field analysis. The Landau theory that we have applied is macroscopic and does not directly indicate the microscopic origin of the phase transitions. As far as this is concerned, there is some evidence that for all three transitions discussed here, the density of total hydrogen bond interactions n_{H-H} increases with decreasing temperature as was described in our previous study [4] and we suggest that this increase is closely connected with the nature of the transitions. As the temperatures of these crystals are lowered, the molecules get closer to one another, thereby establishing more intramolecular and intermolecular hydrogen interactions. When a critical density of the total hydrogen interactions has been established, the phase transition is induced. The reverse process occurs upon raising the temperature, thereby

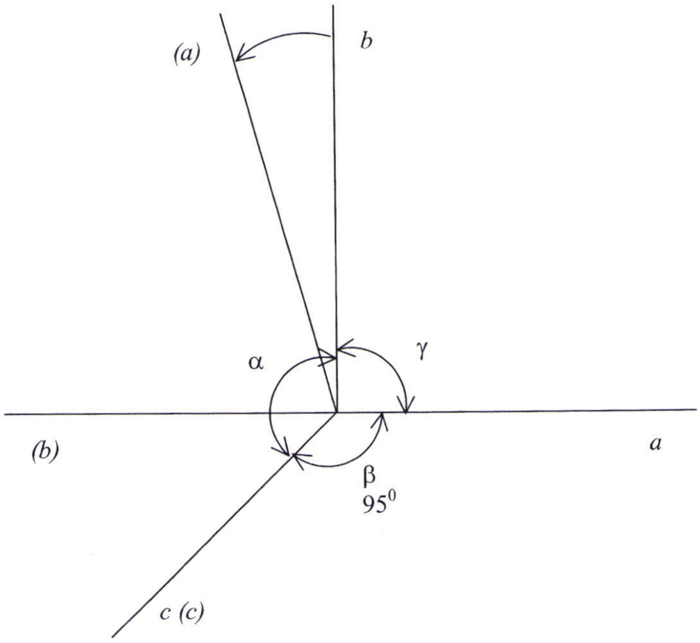

Fig. 4. A sketch showing the monoclinic to triclinic phase transition. The axes are labelled for the monoclinic phase, with triclinic axis labels shown in parenthesis.

explaining the reversible nature of these ferroelastic phase transitions.

What Landau theory can do is to suggest further experiments, and we give two examples. Expressions for the entropy and specific heat may be derived from (1) and [illegible] and we illustrate the method for the orthorhombic-to-monoclinic transitions of Section 2. In a similar way to ferroelectric materials [12,13] the entropy is given by

$$S = -\left(\frac{\partial f}{\partial T}\right)_{u_5} = -\frac{\partial f_0}{\partial T} - \frac{1}{2}Cu_5^2 \tag{11}$$

where (1) and (2) have been used. Substitution of $u_5 = 0$ for $T > T_C$ and of (6) for $T < T_C$ then gives

$$S = -\frac{\partial f_0}{\partial T} \text{ for } T > T_C \tag{12}$$

and

$$S = -\frac{\partial f_0}{\partial T} - \frac{C^2}{2\xi}(T_C - T) \text{ for } T < T_C \tag{13}$$

The entropy is, of course, lower in the ferroelastic phase since it is ordered. The specific heat is $\Gamma = T\frac{\partial S}{\partial T}$, that is,

$$\Gamma = -T\frac{\partial^2 f_0}{\partial T^2} \text{ for } T > T_C \tag{14}$$

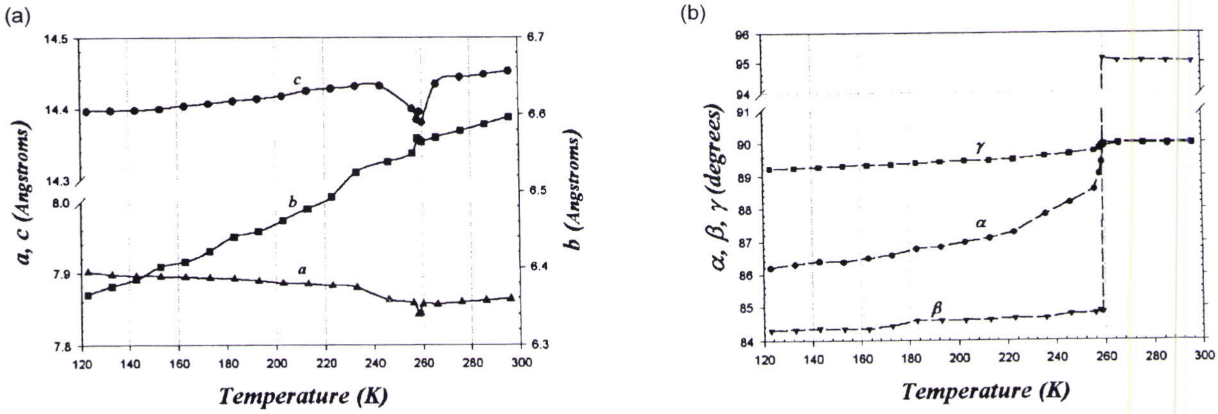

Fig. 5. Temperature dependences of the unit cell parameters of **III**. (a) Unit-cell lengths, (b) unit-cell angles.

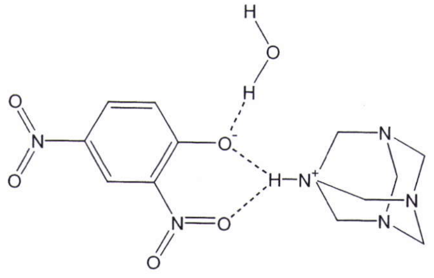

Scheme 3. Schematic diagram of compound **III**.

and

$$\Gamma = -T\frac{\partial^2 f_0}{\partial T^2} + \frac{C^2 T}{2\xi} \text{ for } T < T_C \qquad (15)$$

The second derivative of f_0 may be presumed smoothly varying, so comparison of (14) and (15) shows that at T_c there is a simple discontinuity in Γ equal to $C^2T_C/2\xi$. This is standard for second-order mean-field transitions.

The analysis for the monoclinic-to-triclinic transition is similar, and the formal expressions are the same as above with the relevant ξ and C replaced by B.

As has been seen, the data are consistent with a 'softening' of the elastic stiffness coefficient $c_{55}^{(0)}$ or $c_{44}^{(0)}$. A simple analysis shows that in consequence the velocity of the corresponding acoustic shear wave softens as $v \propto |T - T_C|^{1/2}$. This should be detectable by Brillouin scattering, as should the presumed temperature independence of the other elastic stiffness coefficients.

As in most phase transitions, the low-temperature phase is a state of broken symmetry so that there are degenerate states with the same free energy. In Section 2 the states $\pm u_5$ and in Section 3 the states $\pm u_4$ have the same energy; experimentally this degeneracy may show up in the appearance of domains.

Acknowledgements

We thank the Malaysian Government and Universiti Sains Malaysia for the Fundamental Research Grant: 304/PFIZIK/670011. H.K.F. and S.C. would also like to thank Prof. Claude Lecomte, Université Henri Poincaré, Nancy, France for the data collection resulting in Fig. 5. Additionally HKF thanks EGIDE, France, and SC thanks the Prince of Songkla University, Thailand, for partial financial support.

References

[1] D.M. Blow, Acc. Chem. Res. 9 (1976) 145–156.

[2] E. Fan, C. Vincent, S.J. Geib, A.D. Hamilton, Chem. Mater. 6 (1994) 1113–1117.

[3] G.R. Desiraju, Angew. Chem. Int. Ed. Engl. 34 (1995) 2311–2327.

[4] A. Usman, S. Chantrapromma, H.-K. Fun, Acta Crystallogr. C 57 (2001) 1443–1446.

[5] A. Usman, S. Chantrapromma, H.-K. Fun, B.-L. Poh, C. Karalai, Acta Crystallogr. C 58 (2002) o46–o47.

[6] A. Usman, S. Chantrapromma, H.-K. Fun, B.-L. Poh, C. Karalai, Acta Crystallogr. C 58 (2002) o136–o138.

[7] S. Chantrapromma, A. Usman, H.-K. Fun, B.-L. Poh, C. Karalai, Acta Crystallogr. E 58 (2002) o102–o104.

[8] S. Chantrapromma, A. Usman, H.-K. Fun, B.-L. Poh, C. Karalai, Acta Crystallogr. E 58 (2002) o108–o110.

[9] H.-K. Fun, S. Chantrapromma, A. Usman. The Cambridge Crystallography Data Center, deposition numbers CCDC 177747 and 177748, 2002.

[10] H.-K. Fun, S. Chantrapromma, A. Usman. The Cambridge Crystallography Data Center, deposition numbers CCDC 210835 and 210836, 2003.

[11] S. Chantrapromma, A. Usman, H.-K. Fun, B.-L. Poh, C. Karalai, J. Mole. Struc., in press.

[12] D.R. Tilley, B. Zeks, Solid Status Commun. 49 (1984) 823–827.

[13] L.-H. Ong, J. Osman, D.R. Tilley, Phys. Rev. B 63 (2001) 144109/1–144109/10.

ELSEVIER

Available online at www.sciencedirect.com
SCIENCE DIRECT®

Journal of Molecular Structure 688 (2004) 59–65

Journal of
MOLECULAR
STRUCTURE

www.elsevier.com/locate/molstruc

Structural and spectroscopic studies of the adducts of quinuclidine and 3,5-dinitrobenzoic acid

S. Chantrapromma[a,c], A. Usman[a], H.K. Fun[a,*], B.L. Poh[b], C. Karalai[c]

[a]*School of Physics, Universiti Sains Malaysia, 11800 USM, Penang, Malaysia*
[b]*School of Chemistry, Universiti Sains Malaysia, 11800 USM, Penang, Malaysia*
[c]*Department of Chemistry, Faculty of Science, Prince of Songkla University, Hat-Yai, Songkhla 90112, Thailand*

Received 12 May 2003; revised 26 August 2003; accepted 3 September 2003

Abstract

Two types of adducts of quinuclidine with 3,5-dinitrobenzoic acid, namely quinuclidinium-3,5-dinitrobenzoate and quinuclidinium-3,5-dinitrobenzoate-3,5-dinitrobenzoic acid have been prepared. Their structures were analyzed using X-ray diffraction, FT-IR and ^{1}H NMR spectroscopic methods. In both adducts, there is an H atom transferred from the acid to the quinuclidine N atom creating an ionic pair consisting of the quinuclidinium cation and the 3,5-dinitrobenzoate anion. The N^+–H bond acts as a hydrogen bond donor, whereas the carboxylate group acts as hydrogen bond acceptors.

Keywords: Salt-like adducts; Quinuclidine; 3,5-Dinitrobenzoic acid; Crystal structure; Intermolecular hydrogen bond; FT-IR spectroscopy; ^{1}H NMR spectroscopy

1. Introduction

The adducts of organic acids with amine bases are of interest due to either their hydrogen bond interactions of types O–H···O, O–H···N and N–H···O which are among the robust and versatile synthons in crystal engineering [1,2], or their important role in biological systems [3]. One of the organic acids of interest is a strong acid, 3,5-dinitrobenzoic acid, which readily forms 3,5-dinitrobenzoate anion when co-crystallized with amine bases by transferring an H atom forming salt-like adducts. In these types of adducts, the trigonally 3,5-dinitrobenzoate anion has approximately a non-crystallographic *D3h(2m)* symmetry and is expected to act as a multiple acceptor of hydrogen bonds via the nitro and carboxylate groups.

Recently, we have investigated the interactions between 3,5-dinitrobenzoic acid and several strong amine bases such as hexamethylenetetraamine [4] and piperazine [5]. Their structures were determined by single crystal X-ray diffraction method. We found that the behavior of the amine base in the adducts is co-related to the H-transfer process, whether it is complete or not.

In our ongoing systematic studies on the interactions between 3,5-dinitrobenzoic acid with amine bases, we have selected the quinuclidine as the basic amine since this amine easily forms cation and facilitates a strong attraction between its positively charged N and the negatively charged O atom of the benzoate anion. In this paper, we report the preparation, X-ray structural analyses, FT-IR and ^{1}H NMR spectroscopic studies of two adducts of quinuclidine with 3,5-dinitrobenzoic acid, namely quinuclidinium-3,5-dinitrobenzoate (adduct **I**) and quinuclidinium-3,5-dinitrobenzoate-3,5-dinitrobenzoic acid (adduct **II**) (Fig. 1).

2. Experimental

Both adducts **I** and **II** were prepared by thoroughly mixing of 0.56 g (5 mmol) quinuclidine and 1.06 g (5 mmol) 3,5-dinitrobenzoic acid. The mixture was dissolved in 50 ml of acetone. Distilled water (2 ml) then was added into the mixture to ensure the complete

---

[*] Corresponding author. Tel.: +60-46-533-888x3690; fax: +60-46-579-150.

E-mail address: hkfun@usm.my (H.K. Fun).

0022-2860/$ - see front matter © 2003 Elsevier B.V. All rights reserved.
doi:10.1016/j.molstruc.2003.09.003

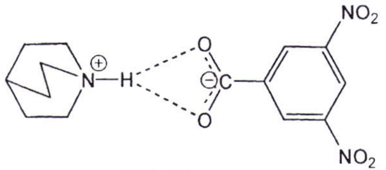

Adduct I

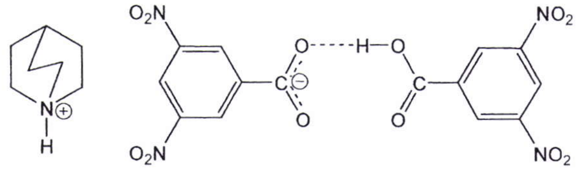

Adduct II

Fig. 1. Schematic diagram of adducts **I** and **II**.

dissolution, and the mixture was warmed-up until a clear solution was obtained. The mixture was then filtered off, and the filtrate was kept at ambient temperature. Slow evaporation of the solvent in air afforded two types of yellow single crystals; needle-like crystals (adduct **I**), and block-like crystals (adduct **II**). All the crystals that have been formed belong to either one or the other morphology. Crystals from each adduct could be easily separated by hand according to the different morphologies. Both adducts were subjected to X-ray structural analyses, FT-IR and ^{1}H NMR spectroscopy and elemental analyses.

Table 1
Summary of crystallographic data and refinement for adducts **I** and **II**

	Adduct **I**	Adduct **II**
Formula	$C_7H_{14}N{\cdot}C_7H_3N_2O_6$	$C_7H_{14}N{\cdot}C_7H_3N_2O_6$ $\cdot C_7H_4N_2O_6$
Formula weight	323.31	535.43
Color; shape	Yellow; needle-like	Yellow; block-like
Crystal system	Monoclinic	Triclinic
Space group	$P2_1/c$	P-1
Z	8	2
Lattice constants	$a = 11.6467$, $b = 23.1900(7)$, and $c = 11.6789(9)$Å, $\alpha = 90$, $\beta = 105.517(1)$, and $\gamma = 90°$	$a = 7.4186(1)$, $b = 13.199(2)$, and $c = 13.315(2)$Å, $\alpha = 71.448(3)$, $\beta = 78.695(4)$, $\gamma = 77.568(3)°$
Volume (Å^3)	3039.4(4)	1195.6(4)
D_x (g cm^{-3})	1.413	1.487
μ (mm^{-1})	0.11	0.12
$F(000)$	1360	556
θ range (deg)	2.4–25.0	2.6–25.0
h, k, l	− 13/13, − 27/26, − 13/8	− 8/8, − 15/15, − 13/15
Reflections collected	14996	5990
Reflections unique	5329	4134
T_{min}/T_{max}	0.957/0.974	0.940/0.976
R(int)	0.024	0.012
Number of parameters	443	361
GoF	1.05	1.07
Final R index ($I > 2\sigma(I)$)	0.061	0.049

Single crystals of both adducts **I** and **II** were cut into proper size and were mounted on glass fibers with epoxy cement for X-ray crystallographic study. The crystallographic data for both adducts at 293 K are gathered in Table 1. The data were collected using a 1 K SMART CCD diffractometer with a graphite monochromated Mo Kα radiation at a detector distance of 5 cm and swing angle of − 35°. A hemisphere of the reciprocal space was cover[illegible] a combination of three sets of exposures using SMART program [6]. Each set had a different φ angle (0, 88, 180°), and each exposure of 30 s covered 0.3° in ω. Coverage of the unique set is over 99% complete for each case. Crystal decay was monitored by repeating thirty initial frames at the end of data collection and analyzing the duplicate reflections, and was found to be negligible. The collected data were reduced using SAINT program [6], and the empirical absorption corrections were preformed using SADABS program [7]. The structures were solved by direct methods and were refined by least-squares using the SHELXTL software package [8]. All non-hydrogen atoms were refined anisotropically, whereas hydrogen atoms were geometrically attached to their parent atoms with ideal bond lengths and angles and were treated as riding atoms, excepting for those hydrogen

Table 2
Selected bond lengths for adducts **I** and **II**

Adduct **I**		Adduct **II**	
Bond	Length	Bond	Length
N(1)–C(1A)	1.426(1)	N(1)–C(1)	1.474(3)
N(1)–C(1B)	1.580(2)	N(1)–C(4)	1.497(4)
N(1)–C(4A)	1.432(7)	N(1)–C(5)	1.481(3)
N(1)–C(4B)	1.453(1)	N(1)–H(1)	0.87(3)
N(1)–C(5)	1.440(5)	O(1)–C(14)	1.253(2)
N(1)–H(1)	0.89(5)	O(2)–C(14)	1.226(3)
N(6)–C(22)	1.482(5)	O(3)–N(2)	1.208(3)
N(6)–C(25)	1.464(5)	O(4)–N(2)	1.209(3)
N(6)–C(27)	1.476(4)	O(5)–N(3)	1.217(2)
N(6)–H(6)	0.91(4)	O(6)–N(3)	1.214(3)
O(1)–C(14)	1.242(4)	O(7)–C(21)	1.203(3)
O(2)–C(14)	1.223(4)	O(8)–C(21)	1.298(3)
O(3)–N(2)	1.211(5)	O(8)–H(81)	1.00(3)
O(4)–N(2)	1.206(5)	O(9)–N(4)	1.215(3)
O(5)–N(3)	1.209(5)	O(10)–N(4)	1.214(2)
O(6)–N(3)	1.213(5)	O(11)–N(5)	1.195(3)
O(7)–C(21)	1.211(4)	O(12A)–N(5)	1.210(1)
O(8)–C(21)	1.259(4)	O(12B)–N(5)	1.228(2)
O(9)–N(4)	1.221(5)		
O(10)–N(4)	1.216(5)		
O(11)–N(5)	1.215(4)		
O(12)–N(5)	1.211(5)		

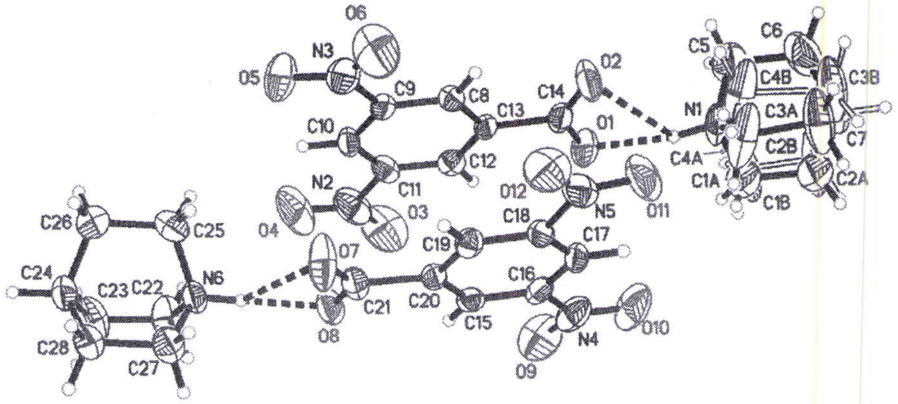

Fig. 2. The structure of the adduct **I** showing 50% probability displacement ellipsoids and the atomic numbering scheme. The broken lines denote the intramolecular interactions. The hydrogen atoms attached to the C atoms have been omitted for the shake of clarity.

atoms, which are involved in hydrogen bonds. These were located from difference Fourier maps and were isotropically refined. As a result of the large fraction of weak data at higher angles, the 2θ maximum was limited to 52° for both adducts **I** and **II**. The final refinement with the conventional R value converged well. The selected bond lengths and angles are represented in Table 2. Materials for publication were prepared using SHELXTL and PLATON [9]. The crystallographic-information files for both adducts have been deposited in the Cambridge Crystallographic Data Base Center as CCDC210139 and CCDC210140, respectively.

The infrared spectra were recorded in solid phase (KBr pellet) and in chloroform solution using a Perkin Elmer 783 FT-IR spectrometer, whereas the ^{1}H NMR spectra were measured using a Varian Unity Inova FT-NMR operating at 500 MHz in $CDCl_3$ solution with TMS as an internal standard. Elemental analyses were performed using a Perkin Elmer elemental analyzer; anal. calcd. for adducts (**I**; mp 167(1) °C, $C_{14}H_{17}N_3O_6$): C, 52.00; H, 5.30; N, 13.00%, found. C, 51.92; H, 5.46; N, 12.89%, and (**II**; mp 249(2) °C, $C_{21}H_{21}N_5O_{12}$): C, 47.10; H, 3.95; N, 13.08%, found. C, 46.95; H, 4.06; N, 12.91%.

3. Results and discussion

Plots of the molecules of both adducts **I** and **II** are shown in Figs. 2 and 3, respectively. The H-transfer process is complete in both adducts. The adduct **I** contains a 1:1 ratio of the quinuclidine and 3,5-dinitrobenzoic acid, the H atom of the acid is transferred to the amine making the complex a salt-like adduct of quinuclidinium-3,5-dinitrobenzoic acid.

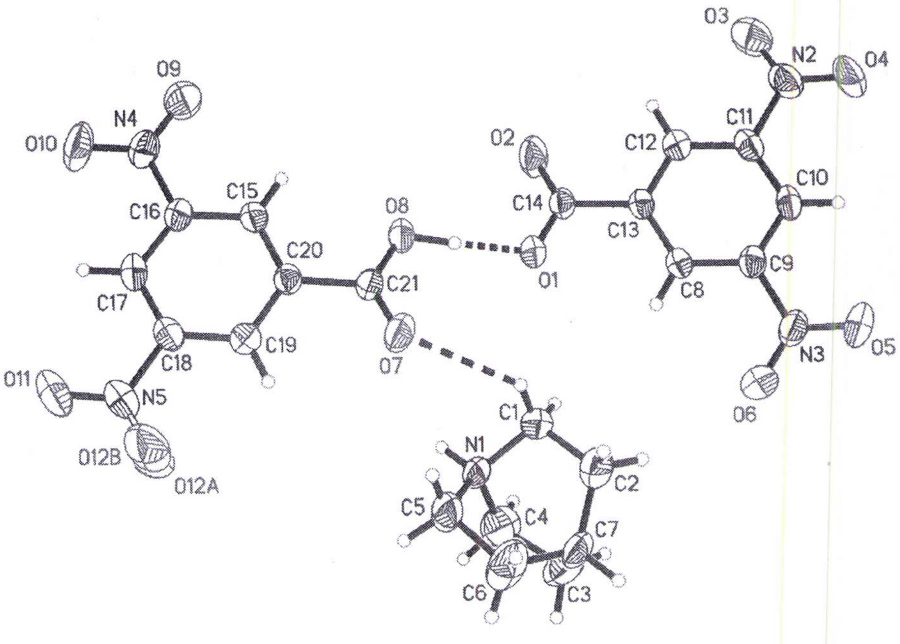

Fig. 3. The structure of the adduct **II** showing 30% probability displacement ellipsoids and the atomic numbering scheme. The broken lines denote the intramolecular interactions.

The two components in the asymmetric unit form two ionic pairs with one of the quinuclidinium cations showing positional disorder.

On the contrary, the adduct **II** contains a 1:2 ratio of the quinuclidine and 3,5-dinitrobenzoic acid, the H atom of one of the acid is transferred to the amine making them a ternary complex, quinuclidinium-3,5-dinitrobenzoate-3,5-dinitrobenzoic acid. Therefore, there are three components, i.e. quinuclidinium cation, 3,5-dinitrobenzoate anion and neutral 3,5-dinitrobenzoic acid. The nitro group O12 atom of the acid also shows positional disorder with the major and minor components (O12A and O12B) deviating oppositely out of the aromatic ring.

The bond lengths and angles in both adducts are within the normal range. Those within the quinuclidinium cation agree with the corresponding values in the related structures

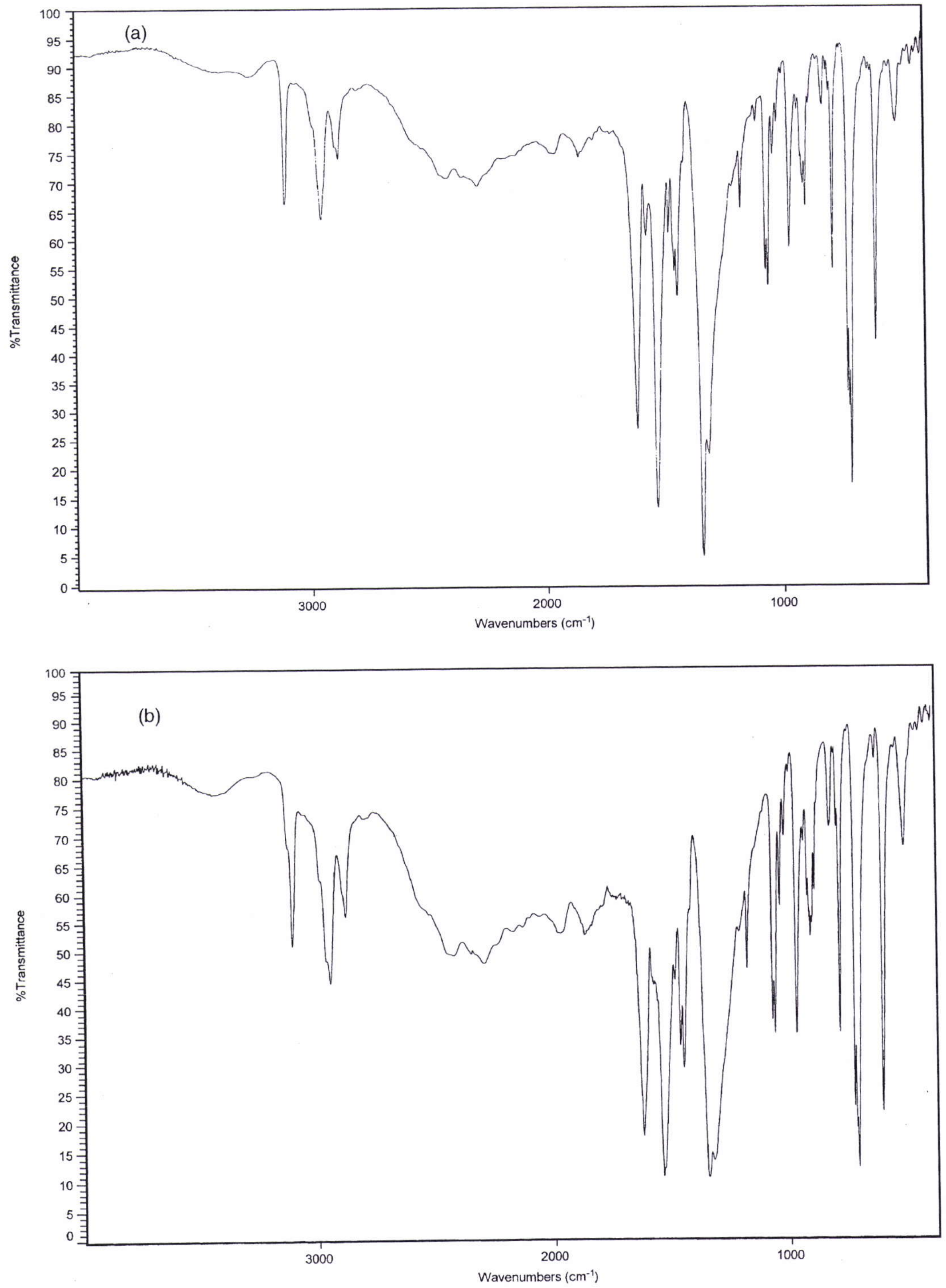

Fig. 4. FT-IR spectra of the adducts **I** and **II** in KBr pellet (a) for adduct **I** and (b) for adduct **II**.

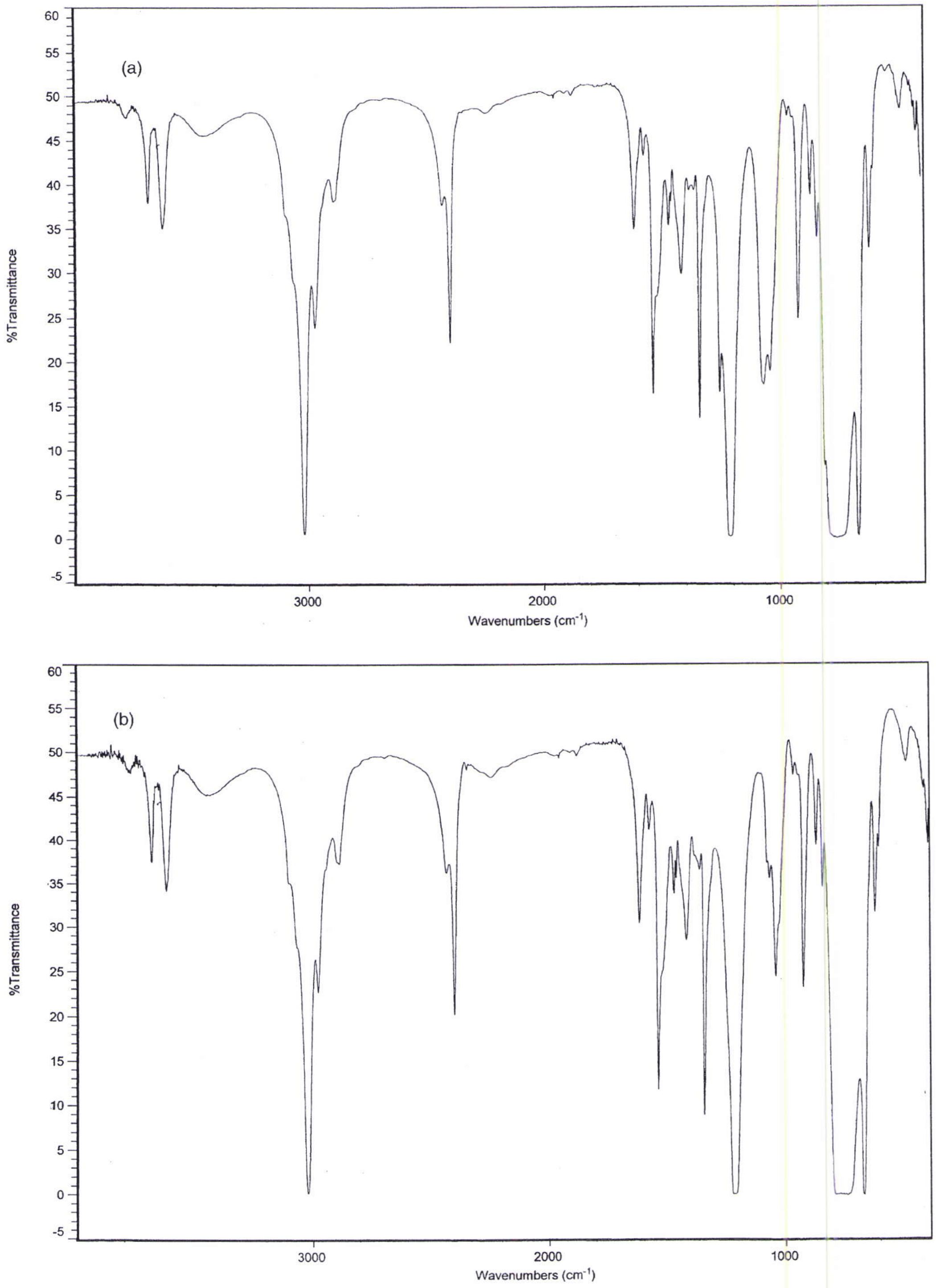

Fig. 5. FT-IR spectra of the adducts **I** and **II** in chloroform (a) for adduct **I** and (b) for adduct **II**.

previously reported such as quinuclidinium diazidotriphenylstannate [10] and quinuclidinium-2,4-dinitrophenolate [4]. Also similar to these structures are the boat conformation of its C–C–C–C–C–N six-membered rings. Additionally, those within the 3,5-dinitrobenzoic acid agree with the previous values reported for the complex of 3,5-dimethylpyridine and 3,5-dinitrobenzoic acid [11].

For both adducts, in addition to the fact that the hydrogen atom transferred to the quinuclidinium N atom was located explicitly from the difference Fourier maps and was freely refined, the quinuclidinium N–C bond distances (Table 2) are those of the typical N–C distances for trimethylammonium cation. The H-transfer process is also supported by the observed N–O, C–N and C–O bond distances of the functional groups which resemble much more the average values for 3,5-dinitrobenzoate anion due to the changes in its π-electron distributions. Particular of this anion structure is the distinct shortening of the C−O bonds and lengthening of the N−O bonds. The bond lengths and angles in this 3,5-dinitrobenzoate anion are consistent with those in its ionic adducts with piperazindiium and hexamethyletetraaminium.

The structures of both adducts are in good agreement with the ^{1}H NMR and IR spectral data. The ^{1}H NMR spectrum of the adduct **I** shows signals δ(ppm) at 9.03 (t, $J = 2$ Hz, 1H) and 9.12 (d, $J = 2$ Hz, 2H) corresponding to the three aromatic protons at positions of 4, 2 and 6, respectively (see the scheme shown in Fig. 1). The signal at 2.20 (septet, $J = 3$ Hz, 1H) is assigned to the methine proton at the C-bridge head of the quinuclidinium skeleton. The other signals at 1.94 (m,6H) and 3.35 (t,6H) correspond to its six methylene attached to the C-bridge head and N-bridge head, respectively. The spectrum of the adduct **II** is similar to that of **I**, excepting the number of the aromatic protons at δ(ppm) 9.19 (t, $J = 2$ Hz, 2H), 9.14 (d, $J = 2$ Hz, 4H), 2.27 (septet, $J = 2$ Hz, 1H), 2.01 (m,6H) and 3.44 (m,6H). The NMR spectra do not show any peak attributable to the iminium proton N−H due to its very weak signal, whereas the spectrum of the adduct **II** shows additional two signals at δ(ppm) 12.79 (br) and 6.13 (br) which could be assignated to carboxyl and ammonium protons, respectively.

In Figs. 4a and b and 5a and b, the FT-IR spectra of adducts **I** and **II** in KBr pellet and chloroform are shown, respectively. In the solid-state spectrum, the bands corresponding to the $\nu_{as}(NO_2)$ and $\nu_s(NO_2)$ vibrations are intense as they appear at 1537 and 1344 cm^{-1} for adduct **I** and 1540 and 1345 cm^{-1} for adduct **II**. The C=O stretching absorption bands of the carboxylate group, $\nu_{as}(CO)$ and $\nu_s(CO)$ appear at 1621 and 1451 cm^{-1} for adduct **I** and at 1623 and 1452 cm^{-1} for adduct **II** where disappearance of absorption band above 1700−1800 cm^{-1} is also observed in adduct **I** (Fig. 4a). These observations are similar to the findings in the complexes of 3,5-dimethylpyridine and 3,5-dinitrobenzoic acid [11]. Based on such similar FT-IR spectra, Johnson and Rumon [12] have suggested that the proton transfer has occurred. This conclusion was confirmed by our X-ray structure determination. More importantly, the intense multiplet band in the 2000−2900 cm^{-1} region implicate proton vibrations at all the hydrogen bonds. The spectra of both adducts in solid phase do not show $\geqslant N^+-H$ stretching, whereas those in chloroform solution phase show clearly the $\geqslant N^+-H$ stretching appearing as sharp peaks at 2397 and 2398 cm^{-1} for adduct **I** and **II**, respectively. The observation of these bands indicates that the protons are localized on the nitrogen atom, i.e. the bands are in correspondence with the proton transfer to quinuclidine, which was found by our X-ray studies. In the FT-IR spectra of the adducts in chloroform solution phase (Fig. 5a and b), a less intense and continuous absorption that extends down to 1700 cm^{-1} and a low-intensity about peak at 1880 cm^{-1} are attrib[illegible] to the medium-strong interactions of the N−H···O hy[illegible]en bonds.

Table 3
Geometries of hydrogen bond interactions in adducts **I** and **II**

	D−H···A	D−H	H···A	D···A	D−H···A
Adduct **I**	N1−H1···O1	0.89(5)	1.86(5)	2.731(6)	171(4)
	N1−H1···O2	0.89(5)	2.57(4)	3.088(5)	118(3)
	N6−H6···O7	0.91(5)	2.59(4)	3.147(4)	120(3)
	N6−H6···O8	0.91(5)	1.76(4)	2.674(4)	177(4)
Adduct **II**	N1−H1···O2^i	0.87(3)	1.92(3)	2.724(3)	152(3)
	O8−H81···O1	1.00(3)	1.52(3)	2.512(2)	175(4)
	C1−H1B···O7	0.97	2.45	3.216(4)	135(3)

Symmetry code: $i = -x,\ 1 - y,\ 1 - z$.

In the X-ray structure analyses, it was found that the hydrogen bonds in both adducts are mainly N−H···O and O−H···O interactions, as expected (Table 3). The D−H distances in Table 3 are distances between electron density maxima and therefore foreshortened as normally observed in X-ray studies. In the asymmetric unit of adduct **I**, each of the two ionic pairs, quinuclidinium cation and 3,5-dinitrobenzoate anion, are linked by two N−H···O hydrogen bonds. In this manner, the N−H bonds facilitate bifurcated systems with the O atoms of the carboxylate group, and the anions act as acceptor of the hydrogen bonds. In the packing, the molecules are interconnected into chains by C−H···O interactions.

In the asymmetric unit of adduct **II**, the 3,5-dinitrobenzoate anion and neutral 3,5-dinitrobenzoic acid are linked by O8−H81···O1 hydrogen bond, and the acid is interconnected to the quinuclidinium cation by C1−H1B···O7 [illegible] interaction. The molecules are interconnected into colu[illegible] stabilized by N1−H1···O2 hydrogen bonds. Its molecular packing is built from these columns.

The intermolecular hydrogen bonds and the ionic interactions in both adducts **I** and **II** are the reasons for the relatively high melting points of their crystals. These are also believed to be favorable factors for the formation of relatively high numbers of the crystals with large sizes during crystallization.

Acknowledgements

This work was supported by the Fundamental Research Grant: R&D No. 304/PFIZIK/670011 from Malaysian Government and Universiti Sains Malaysia.

References

[1] E. Fan, C. Vincent, S.J. Geib, A.D. Hamilton, Chem. Mater. 6 (1994) 1113.

[2] G.R. Desiraju, Angew. Chem. Int. Ed. Engl. 34 (1995) 2311.

[3] D.M. Blow, Acc. Chem. Res. 9 (1976) 145.

[4] (a) H.-K. Fun, A. Usman, S. Chantrapromma, J. Osman, L.-H. Ong, D.R. Tilley, Y. Ishibashi, Solid State Commun. 127 (2003) 677.
(b) A. Usman, S. Chantrapromma, H.-K. Fun, Acta Crystallogr. C 57 (2001) 1443.

[5] A. Usman, S. Chantrapromma, H.-K. Fun, B.-L. Poh, C. Karalai, Acta Crystallogr. C 58 (2002) o136.

[6] Siemens, SMART and SAINT, Siemens Analytical X-ray Instruments Inc., Madison, WI, 1997.

[7] G.M. Sheldrick, SADABS. Program for Empirical Absorption of Area Detector Data, University of Göttingen, Germany, 1996.

[8] G.M. Sheldrick, SHELXTL V5.1, Bruker AXS Inc., Madison, WI, 1997.

[9] A.L. Spek, Acta Crystallogr. A 46 (1990) C-34.

[10] I. Wharf, R. Wojtowski, M. Onyszchuck, M.G. Simard, Acta Crystallogr. C 53 (1997) 1791.

[11] L.B. Jerzykiewicz, Z. Malarski, L. Sobczyk, T. Lis, E. Grech, J. Mol. Struct. 440 (1998) 175.

[12] S.L. Johnson, K.A. Rumon, J. Phys. Chem. 69 (1965) 74.

Acta Crystallographica Section E
Structure Reports
Online
ISSN 1600-5368
Editors: **W. Clegg and D. G. Watson**

1,4-Diazabicyclo[2.2.2]octanium bis(3,5-dinitrobenzoate) monohydrate

Suchada Chantrapromma and Hoong-Kun Fun

Acta Crystallographica Section E
Structure Reports
Online
ISSN 1600-5368

1,4-Diazabicyclo[2.2.2]octanium bis(3,5-dinitrobenzoate) monohydrate

Suchada Chantrapromma‡ and Hoong-Kun Fun*

X-ray Crystallography Unit, School of Physics, Universiti Sains Malaysia, 11800 USM, Penang, Malaysia

‡ Additional correspondence author. Permanent address: Department of Chemistry, Faculty of Science, Prince of Songkla University, Hat-Yai, Songkhla 90112, Thailand

Correspondence e-mail: hkfun@usm.my

Received 4 June 2004
Accepted 21 June 2004
Online 26 June 2004

The title compound, $C_6H_{14}N_2^{2+}\cdot 2C_7H_3N_2O_6^-\cdot H_2O$, is a monohydrate of a 1:2 hydrate adduct of 1,4-diazabicyclo[2.2.2]octane (DABCO) and 3,5-dinitrobenzoic acid. The $(DABCOH_2)^{2+}$ cation adopts the role of a donor in intermolecular N—H···O hydrogen bonding, while both the 3,5-dinitrobenzoate anions act as multiple acceptors of N—H···O, O—H···O and C—H···O hydrogen bonds. These hydrogen bonds result in the formation of a three-dimensional network.

Key indicators

Single-crystal X-ray study
T = 183 K
Mean σ(C–C) = 0.004 Å
R factor = 0.053
wR factor = 0.128
Data-to-parameter ratio = 11.0

For details of how these key indicators were automatically derived from the article, see http://journals.iucr.org/e.

Comment

Interactions of organic acids with amine bases in the solid phase have been of interest due to their hydrogen-bonding interactions (Coupar *et al.*, 1997; Sobczyk *et al.*, 2000) and their important role in biological systems (Blow, 1976). Among the organic acids, 3,5-dinitrobenzoic acid is of interest since it readily forms the 3,5-dinitrobenzoate anion when co-crystallized with amine bases by transferring a proton. This proton transfer leads to the formation of salt-like adducts consisting of 3,5-dinitrobenzoate anions and amine-based cations in which the 3,5-dinitobenzoate anion is expected to act as a multiple acceptor of hydrogen bonds *via* nitro and carboxylate groups.

Owing to this interest, we have investigated recently the interaction between 3,5-dinitrobenzoic acid with several amine bases such as 2,4′-bipyridine (Chantrapromma *et al.*, 2002*a*), quinuclidine (Chantrapromma,Usman, Fun, Poh & Karalai, 2004) and hexamethylenetetramine (Fun *et al.*, 2003; Chantrapromma, Usman & Fun, 2004). The proton transfer process occurs in these adducts and the adduct of 3,5-dinitrobenzoic acid with hexamethylenetetramine undergoes a phase transition (Fun *et al.*, 2003). In our ongoing systematic studies on the interactions between 3,5-dinitrobenzoic acid and amine bases, the title compound, (I), was prepared.

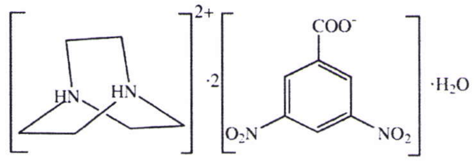

(I)

The asymmetric unit of (I) (Fig. 1) comprises one 1,4-diazabicyclo[2.2.2]octanium dication, $[HN(CH_2CH_2)_3NH]^{2+}$ or $(DABCOH_2)^{2+}$, two 3,5-dinitrobenzote anions and one water molecule. Each molecule of 3,5-dinitrobenzoic acid has transferred a proton from its carboxyl group to an N atom of

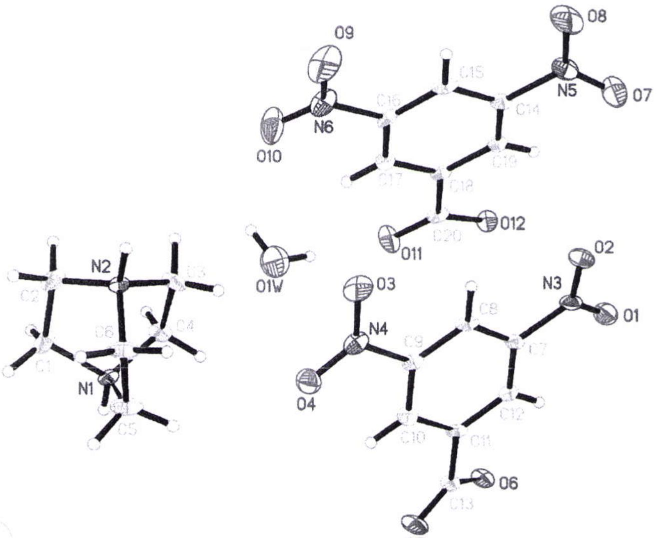

Figure 1

The asymmetric unit of the title compound, showing 50% probability displacement ellipsoids and the atomic numbering scheme.

DABCO which, together with the water molecule, has resulted in the asymmetric unit being a hydrated salt.

This protonation process is accompanied by an increase in the N—C bond distances around these N atoms [average N—C bond distance is 1.492 (4) Å]. These N—C bond distances agree with the mean value of 1.502 (15) Å reported for C—N$^+$ bonds by Allen *et al.* (1987). The protonated N—C bonds in the doubly protonated (DABCOH$_2$)$^{2+}$ are comparable with the protonated N—C bond in the singly protonated (DABCOH)$^+$ cation (Chantrapromma *et al.*, 2002*b*; Ferguson *et al.*, 1997).

The N—C—C—N—C—C six-membered rings of the (DABCOH$_2$)$^{2+}$ cation adopt a slightly twisted boat conformation with puckering parameters (Cremer & Pople, 1975) Q = 0.827 (3) Å, θ = 89.9 (2)° and φ = 348.4 (2)° for the N1/C1/C2/N2/C3/C4 ring, Q = 0.832 (3) Å, θ = 90.1 (2)° and φ = 191.6 (2)° for the N1/C1/C2/N2/C6/C5 ring, and Q = 0.825 (3) Å, θ = 89.7 (2)° and φ = 348.3 (2)° for the N1/C4/C3/N2/C6/C5 ring. The bond lengths and angles within the two symmetry-independent 3,5-dinitrobenzoate anions are comparable and both molecules are nearly planar. The geometric parameters in the 3,5-dinitrobenzoate anion are also comparable with the corresponding values in its adducts with quinuclidine (Chantrapromma, Usman, Fun, Poh & Karalai, 2004).

In the crystal structure of (I) (Fig. 2), the (DABCOH$_2$)$^{2+}$ cation and 3,5-dinitrobenzoate anions are linked by intermolecular N—H···O hydrogen bonds (Table 2), with the (DABCOH$_2$)$^{2+}$ cation acting as a donor. The carboxylate O atoms act as acceptors of intermolecular O—H···O hydrogen bonds with the water molecules. In addition to the electrostatic, N—H···O and O—H···O interactions, the crystal structure is also stabilized by C—H···O interactions (Table 2). These interactions link the ions and water molecules into a three-dimensional network.

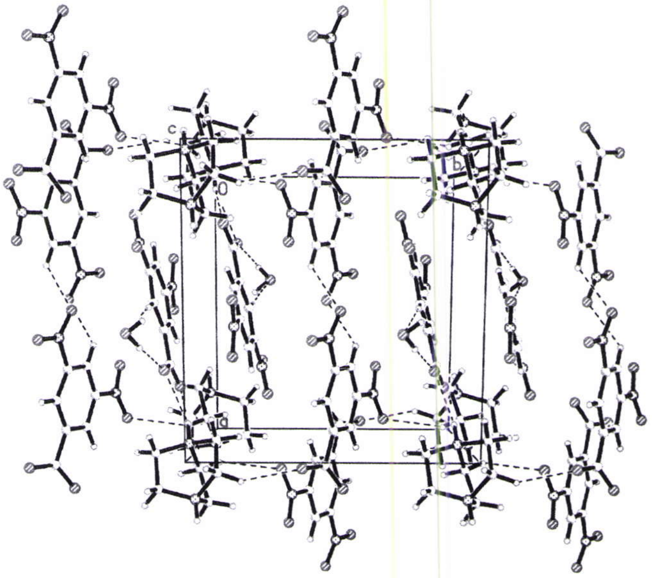

Figure 2

Packing diagram of the title compound, viewed down the *c* axis, illustrating the intermolecular hydrogen bonds (dashed lines).

Experimental

Equimolar amounts of 1,4-diazabicyclo[2.2.2]octane (0.34 g, 3 mmol) and 3,5-dinitrobenzoic acid (0.64 g, 3 mmol) were mixed and dissolved in ethanol (50 ml), with addition of 4 ml of distilled water, and the mixture was warmed to the temperature range 328–333 K until a clear solution was obtained. The solution was then filtered and the filtrate was left to evaporate slowly in air. Colorless single crystals, suitable for X-ray diffraction studies, were obtained from the solution after a few days [m.p. 547–548 K (decomposition)].

Crystal data

$C_6H_{14}N_2^{2+}\cdot 2C_7H_3N_2O_6^{-}\cdot H_2O$
M_r = 554.44
Monoclinic, $P2_1/n$
a = 11.6505 (5) Å
b = 10.4942 (5) Å
c = 19.4752 (9) Å
β = 104.799 (1)°
V = 2302.10 (18) Å^3
Z = 4

D_x = 1.600 Mg m^{-3}
Mo *Kα* radiation
Cell parameters from 10514 reflections
θ = 2.7–25.0°
μ = 0.14 mm^{-1}
T = 183 (2) K
Block, colorless
0.44 × 0.32 × 0.16 mm

Data collection

Bruker SMART CCD area-detector
ω scans
Absorption correction: multi-scan (*SADABS*; Sheldrick, 1996)
$T_{\min}$ = 0.943, $T_{\max}$ = 0.979
10 514 measured reflections
3987 independent reflections

2527 reflections with $I > 2\sigma(I)$
$R_{\rm int}$ = 0.076
$\theta_{\max}$ = 25.0°
$h = -13 \rightarrow 13$
$k = -12 \rightarrow 12$
$l = -20 \rightarrow 23$

Refinement

Refinement on F^2
$R[F^2 > 2\sigma(F^2)] = 0.053$
$wR(F^2) = 0.128$
S = 0.94
3987 reflections
367 parameters
H atoms treated by a mixture of independent and constrained refinement

$w = 1/[\sigma^2(F_o^2) + (0.0309P)^2]$ where $P = (F_o^2 + 2F_c^2)/3$
$(\Delta/\sigma)_{\max} < 0.001$
$\Delta\rho_{\max}$ = 0.38 e Å^{-3}
$\Delta\rho_{\min}$ = −0.44 e Å^{-3}
Extinction correction: *SHELXTL*
Extinction coefficient: 0.0103 (11)

Table 1
Selected geometric parameters (Å, °).

O5—C13	1.238 (3)	N2—C6	1.488 (4)
O6—C13	1.286 (3)	N2—C2	1.490 (3)
O11—C20	1.234 (3)	N3—C7	1.473 (3)
O12—C20	1.283 (3)	N4—C9	1.482 (3)
N1—C4	1.491 (3)	N5—C14	1.473 (4)
N1—C5	1.497 (3)	N6—C16	1.482 (3)
N1—C1	1.497 (3)	C11—C13	1.521 (4)
N2—C3	1.487 (3)	C18—C20	1.529 (4)
O5—C13—O6	125.6 (3)	O11—C20—O12	125.4 (3)
O6—C13—C11	114.3 (2)	O12—C20—C18	115.7 (2)

Table 2
Hydrogen-bonding geometry (Å, °).

D—H⋯A	D—H	H⋯A	D⋯A	D—H⋯A
N1—H1N1⋯O11^{i}	0.94 (1)	2.56 (2)	3.119 (3)	118 (2)
N1—H1N1⋯O12^{i}	0.94 (1)	1.72 (2)	2.658 (3)	174 (3)
N2—H1N2⋯O6^{ii}	0.94 (1)	1.63 (3)	2.566 (3)	174 (4)
O1W—H1W1⋯O5^{iii}	0.90 (1)	1.97 (3)	2.823 (3)	156 (3)
O1W—H2W1⋯O11	0.91 (1)	1.95 (3)	2.839 (3)	168 (3)
C1—H1B⋯O1^{iv}	0.99	2.50	3.332 (4)	141
C3—H3A⋯O4	0.99	2.60	3.409 (3)	139
C3—H3B⋯O5^{iii}	0.99	2.43	3.306 (4)	148
C6—H6B⋯O2^{v}	0.99	2.51	3.397 (4)	149
C6—H6B⋯O7^{v}	0.99	2.54	3.189 (4)	123
C8—H8⋯O3^{v}	0.95	2.49	3.264 (3)	138
C17—H17⋯O1W	0.95	2.41	3.315 (4)	160

Symmetry codes: (i) $\frac{1}{2}-x, \frac{1}{2}+y, \frac{1}{2}-z$; (ii) $x-1, y, z$; (iii) $\frac{1}{2}-x, y-\frac{1}{2}, \frac{1}{2}-z$; (iv) $x-\frac{1}{2}, \frac{3}{2}-y, \frac{1}{2}+z$; (v) $-x, 2-y, -z$.

H atoms of the water molecule and the H atoms attached to atoms N1 and N2 were located in a difference map. They were refined isotropically with the O—H and H⋯H distances restrained to 0.89 (1) and 1.39 (1) Å, respectively, and with N—H = 0.93 (1) Å. The remaining H atoms were positioned geometrically (C—H = 0.95–0.99 Å) and allowed to ride on their parent C atoms, with $U_{iso}(H) = 1.2U_{eq}(C)$.

Data collection: *SMART* (Siemens, 1996); cell refinement: *SAINT* (Siemens, 1996); data reduction: *SAINT*; program(s) used to solve structure: *SHELXTL* (Sheldrick, 1997); program(s) used to refine structure: *SHELXTL*; molecular graphics: *SHELXTL*; software used to prepare material for publication: *SHELXTL* and *PLATON* (Spek, 2003).

SC thanks Prince of Songkla University for partial financial support. The authors thank the Malaysian Government and Universiti Sains Malaysia for research grant R&D No. 304/PFIZIK/670011.

References

Allen, F. H., Kennard, O., Watson, D. G., Brammer, L., Orpen, A. G. & Taylor, R. (1987). *J. Chem. Soc. Perkin Trans.* 2, pp. S1–19.

Blow, D. M. (1976). *Acc. Chem. Res.* **9**, 145–156.

Chantrapromma, S., Usman, A. & Fun, H.-K. (2004). *J. Mol. Struct.* Accepted.

Chantrapromma, S., Usman, A., Fun, H.-K., Poh, B. L. & Karalai, C. (2002*a*). *Acta Cryst.* C**58**, o589–o590.

Chantrapromma, S., Usman, A., Fun, H.-K., Poh, B. L. & Karalai, C. (2002*b*). *Acta Cryst.* C**58**, o102–o104.

Chantrapromma, S., Usman, A., Fun, H. K., Poh, B. L. & Karalai, C. (2004). *J. Mol. Struct.*, **688**, 59–65.

Coupar, P. I., Glidewell, C. & Ferguson, G. (1997). *Acta Cryst.* B**53**, 521–533.

Cremer, D. & Pople, J. A. (1975). *J. Am. Chem. Soc.* **97**, 1354–1358.

Ferguson, G., Bell, W., Coupar, P. I. & Glidewell, C. (1997). *Acta Cryst.* B**53**, 534–543.

Fun, H.-K., Usman, A., Chantrapromma, S., Osman, J., Ong, L. H., Tilly, D. R. & Ishibashi, Y. (2003). *Solid State Commun.* **127**, 677–682.

Sheldrick, G. M. (1996). *SADABS*. University of Göttingen, Germany.

Sheldrick, G. M. (1997). *SHELXTL*. Version. 5.1. Bruker AXS Inc., Madison, Wisconsin, USA.

Siemens (1996). *SMART* and *SAINT*. Siemens Analytical X-ray Instruments Inc., Madison, Wisconsin, USA.

Sobczyk, L., Lis, T., Olejnik, Z. & Majerz, I. (2000). *J. Mol. Struct.* **552**, 233–241.

Spek, A. L. (2003). *J. Appl. Cryst.* **36**, 7–13.

Microscopic theory of phase transitions in hydrogen–bonded phenol–amine adducts

Pye Ton How

School of Physics, Universiti Sains Malaysia, 11800 USM Penang, Malaysia

Beck Sim Lee

INTI International College, Penang, Malaysia

Hoong-Kun Fun

School of Physics, Universiti Sains Malaysia, 11800 USM Penang, Malaysia[*]

Ibrahim Abdul Razak

School of Physics, Universiti Sains Malaysia, 11800 USM Penang, Malaysia

Suchada Chantrapromma

School of Physics, Universiti Sains Malaysia, 11800 USM Penang, Malaysia[†]

(Dated: March 29, 2004)

Second-order reversible ferroelastic phase transitions in a recently discovered class of hydrogen-bonded phenol-amine adducts has already been analysed by Landau theory. The analysis is however phenomenological and does not directly indicate the microscopic origin of this phase transition. In this paper, a microscopic theory is presented. It is proposed that the main mechanism responsible for the phase transition is the interaction of hydrogen bonds with the lattice vibrations or phonons of the crystal. These interactions with the phonons induce long range cooperative interactions between the hydrogen bonds, which causes the phase transition behavior at the critical temperature. Critical exponents for unit cell parameters and heat capacity are derived with a variational meanfield approach, and shown to be consistent with the prediction of Landau's theory.

PACS numbers: 63.70.+h, 63.20.LS, 61.50.KS